ISSN 0280-5316
ISRN LUTFD2/TFRT--5772--SE

All Wheel Drive Hardware Dependant Control

Jennie Malm

Department of Automatic Control
Lund University
June 2006

Department of Automatic Control
Lund Institute of Technology
Box 118
SE-221 00 Lund Sweden

Document name
MASTER THESIS

Date of issue
June 2006

Document Number
ISRNLUTFD2/TFRT--5772--SE

Author(s)
Jennie Malm

Supervisor
Anders Rantzer at Automatic Control in Lund, Sweden
Edo F Drenth at Haldex in Landskrona, Sweden

Sponsoring organization

Title and subtitle
All Wheele Drive Hardware Dependant Control. (Hårdvaruberoende reglering av fyrhjulsdrift)

Abstract
Haldex Traction AB designs and manufactures an all wheel drive system called *Haldex Limited Slip Coupling*. A slip controller controls the speed differences between the front and rear shafts in the all wheel drive vehicle. The product exists in three generations and a fourth, with some major hardware differences, is under development. The variations in hardware lead to widely different demands on the control software of the slip controller. This master thesis presents a well-founded comparison between Generation I and IV from a control design perspective.
Two models were made of the coupling, one for the two generations respectively, and simulated together with a simple vehicle model and a PID controller. The control parameters were tuned for a normal driving condition and then tested for different disturbances. The simulations show that the slip controller in Generation IV can be made faster due to less embedded delay in the coupling. Generation I on the other side is more robust to changes in friction between the tyres and the surface and is more stable for time delays from the CANbus.

Keywords

Classification system and/or index terms (if any)

Supplementary bibliographical information

ISSN and key title
0280-5316

ISBN

Language
English

Number of page
72

Recipient's notes

Security classification

Acknowledgements

Many people have contributed to this master thesis and I want to thank all of them for giving me their time, assistance and patience so generously.

First of all, I would like to thank my supervisors Edo Drenth at Haldex Traction AB and Anders Rantzer at the Department of Automatic Control at Lund Institute of Technology. Thanks to Edo Drenth for giving me the opportunity to perform my master thesis at Haldex Traction AB, for helping me understand vehicle dynamics and for providing me with usable information. Thanks to Anders Rantzer for giving me advice in both practical and theoretical problems with my master thesis and for giving me recommendations on people to contact with further problems.

I also want to thank Magnus Gäfvert at Modelon AB for helping me with the vehicle model used in the simulations and for making sure the results were realistic. Thanks to Jacob Svendenius for his help with control theory related problems and for providing me with new ideas when I got stuck. I would also like to thank research assistant and PhD Anders Robertsson at the Department of Automatic Control at Lund Institute of Technology for his help with the linearization of the vehicle model.

Special thanks to all the employees at Haldex Traction AB for making this spring a memorable and educational time for me.

Finally, I would like to thank my friends and family for their patience during this time and for helping me with proofreading and giving me valuable comments.

June 2006

Jennie Malm

Contents

1 Introduction

In the introduction chapter the objectives and structure of the master thesis are presented and motivated. Furthermore the boundaries and target groups are defined. Finally the outline of the report is presented and each chapter is introduced to the reader.

1.1 Background

Haldex Traction AB designs and manufactures an all wheel drive system called Haldex Limited Slip Coupling. At present time the fourth generation, a more cost efficient version of the product, is being developed. There are major hardware differences between the generations which lead to widely different demands on the control software.

1.2 Purpose

The purpose of this master thesis is to compare the slip controllers between the Haldex Limited Slip Coupling Generation I and Generation IV by simulating them in a vehicle model.

1.3 Goal

The goal is to present a well-founded comparison between the slip controllers in Generation I and IV from a control design perspective.

1.4 Achievements

Two Matlab/Simulink models with a vehicle, a PID controller and the two couplings respectively have been built up from the bottom. The models were then altered to introduce disturbances to the system. Tools to simplify and systemize the tuning of the control parameters have been developed. This includes a Matlab script for generating tuning maps and programs that calculate error quantifications for different disturbances to the system. The work has lead to a documented comparison between Generation I and IV.

1.5 Boundaries

Since timing does not allow real verifications in a wintry environment the comparison between the coupling in Generation I and Generation IV has been restricted to simulations. For this purpose a simplified vehicle model was build. The simplifications include, e.g., using a bicycle model driving straight ahead and not modelling a gear box.

1.6 Target Group

This report is mainly intended for employees at Haldex Traction AB who are well-informed on the issues handled in this thesis. Secondly the report is intended for engineering students in the end phase of their education. The language is therefore adapted to their level. Knowledge of the Haldex Traction AB product and vehicle dynamics is not needed to understand this report since these are introduced in the following text.

1.7 Outline

The report starts with a theory chapter on vehicle dynamics. A simple introduction to the vehicular driveline gives the reader the basic knowledge needed to understand the vehicle dynamics notations used in this report. The Haldex Traction AB all wheel drive system *Haldex Limited Slip Coupling* is explained with a focus on describing the differences between

Generation I and Generation IV. In this chapter the equations that determine the motion of the vehicle as well as basic notations of wheel and tyre dynamics are introduced and explained.

In the next chapter the specifications on the slip controllers are presented and methods used to quantify and evaluate deviations from the desired value are introduced. The simulation models build in Matlab/Simulink to verify the slip controllers are explained, first in general and then for each block separately. Next, the control design process is described. This includes a linearization of the vehicle model, some control theory used in the thesis and the actual tuning of the control parameters. Finally some comments on the simulations and the implementations are found.

In the fourth chapter the requirements on the slip controllers are outlined and the simulations performed to evaluate these are listed. Thereafter the results from the simulations are discussed separately for Generation I and IV.

The conclusions are found in the fifth chapter. Here the comparison between the slip controllers done in chapter four is presented.

The notations used in the report are listed in Appendix A, this includes symbols and abbreviations. A glossary is found in Appendix B. Finally, in Appendix C, the Matlab/Simulink program for the simulation model is shown.

2 Vehicle Dynamics

This chapter begins with a brief introduction to the vehicular driveline, intended for the reader who is unfamiliar with vehicle dynamics. The Haldex Traction AB all wheel drive system will then be explained briefly. This is followed by an explanation of the equations of motion which will be used in the report. Finally basic notations of wheel and tyre dynamics are introduced.

2.1 Vehicle Driveline

The *driveline* denotes the parts of the vehicle that makes the vehicle drive forward. It includes the engine, the clutch, the transmission, the shafts and the wheels. A schematic presentation of the driveline of a rear wheel drive car is shown in Figure 2.1. The *engine* generates a rotational movement which is translated into driving torque in the *transmission*. This allows the engine to work at fairly constant rotational speed for different vehicle velocity. The transmission has a set of gears with different conversion ratios, depending on the desired vehicle velocity and traction force different gear ratios are used. Decreased velocity allows an increased traction force on a low gear, and contrariwise. There is also a reverse gear which reverses the direction of rotation, making the driving wheels turn backwards. For a rear wheel driven vehicle the *drive shaft* connects the final drive with the wheels. [1]

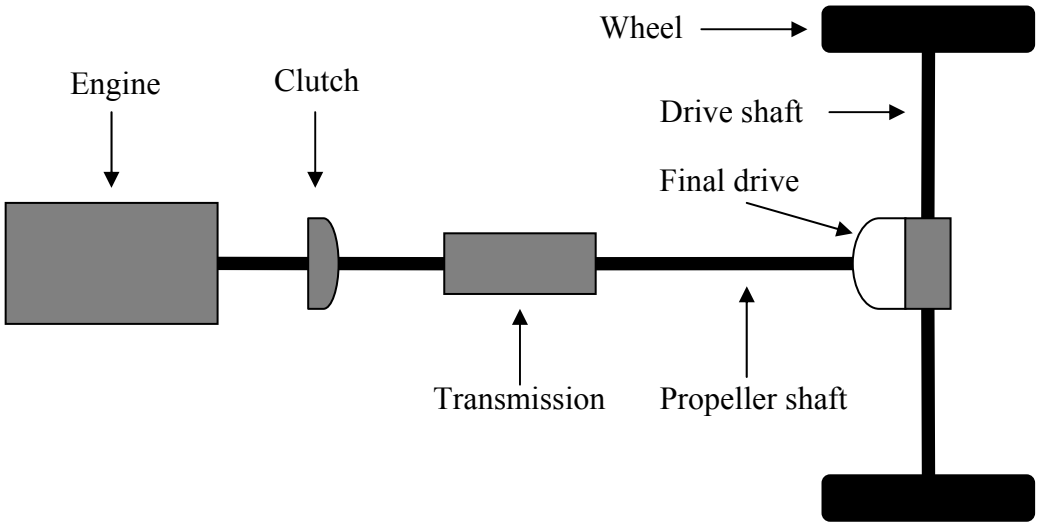

Figure 2.1 Vehicular driveline for a rear driven vehicle [1].

To be able to turn a car smoothly it has to have a *differential* which allows the outer wheel to turn faster, enabling it to travel a longer distance than the inner wheel. The differential transfers power to the wheel that moves the easiest. This can lead to problems if one wheel is on a slippery surface. The wheel on the slippery surface will start spinning while the other one will not. To avoid this behaviour an all wheel drive system divides torque between the four wheels and hence getting as much power to the ground as possible. [1]

The term *all wheel drive* (AWD) is often used to classify vehicles that automatically switch from two wheel drive to four wheel drive when needed. AWD was introduced to distinguish these vehicles from so called *four wheel drive* (4WD or 4x4) vehicles with permanent four wheel driving or where the driver manually has to switch between two and four wheel driving. The market for AWD-systems is increasing rapidly. Of the today produced cars about 10 % have some kind of all wheel drive system. [2]

2.2 Haldex Limited Slip Coupling

One of the AWD-systems available on the market is the Haldex Limited Slip Coupling (HLSC). It was invented by Sigvard Johansson who was a Swedish rally driver in the 1960s. He wanted to create a manual hydraulic mechanical limited slip differential to avoid manual configuration before each race. In 1988 this resulted in a patent which was bought by Haldex AB four years later. [3]

The HLSC has the advantage of being compatible with systems like brake control ABS (Anti-lock Braking System), traction control TCS (Traction Control System) and stability control ESP (Electronic Stability Program) because of its total controllability and its reaction speed. [4]

The coupling now exists in three generations and a fourth is under development and is planned to go into production 2007 [2]. Generation I and II have the same basic structure. In the master thesis Generation IV was compared to Generation I because of its mathematical simplicity.

2.2.1 Basic Function of HLSC Generation I

Figure 2.2 shows a simplified sketch of a HLSC Generation I. To transform a front wheel drive vehicle to an all wheel drive the ingoing shaft (left in the figure) is connected to the front differential, the gear box and the engine and the outgoing shaft (right in the figure) is connected to the rear differential. The wet multi-plate clutch consists of discs where every second disc is connected to the ingoing shaft and the other discs are connected to the outgoing shaft. [5]

When the front and rear shafts of the vehicle start to rotate with different velocities, e.g., due to slip, the hydraulic piston pump will start to rotate generating an oil flow through the open throttle valve. When the throttle valve, which is controlled by a stepping motor, is partially closed an oil pressure will start to build up in the clutch piston. The clutch piston will force the discs in the multi-plate clutch together which leads to a torque capacity from the front to the rear shaft. The torque transferred in the coupling is a function of the pressure. The goal is hence to control the pressure in the clutch in order to be able to control the torque transfer. However, the pressure can not be directly controlled but depends on the position of the controllable throttle valve and the difference in angular velocity between the front and the rear shaft. The transferred torque is therefore not a linear function of the throttle valve position. [6]

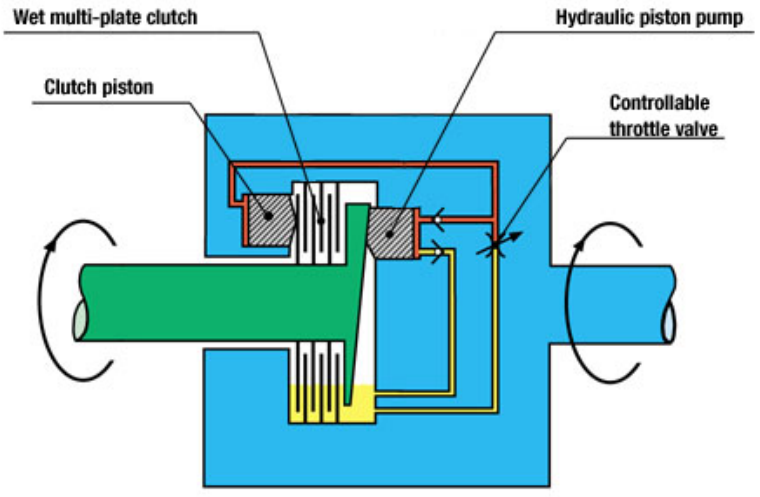

Figure 2.2 Basic structure of the Haldex Limited Slip Coupling for Generation I [4].

The control signal in the system is called *stiffness* and is defined as

$$\delta = \frac{P}{Q} \tag{2.1}$$

where P is the pressure in the clutch piston and Q the oil flow produced by the hydraulic piston pump, see Figure 2.3. Depending on the value of δ a specific flow will hence give different pressure in the clutch piston. [7]

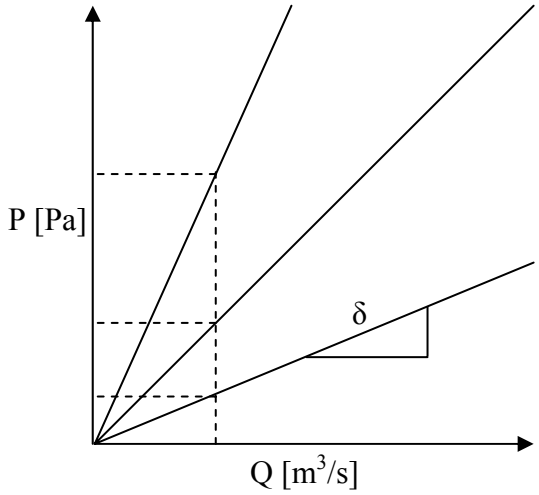

Figure 2.3 The pressure in the clutch piston as a function of the oil flow produced by the hydraulic piston pump.

Information about, e.g., the engine, the brakes and individual wheel velocities are read into a microprocessor in the HLSC and processed in a control program that controls the coupling. The microprocessor is connected to the CAN-bus, the communication system of the vehicle. [4]

The oil flow is calculated from the difference in angular velocity between the front and rear shaft, which are received from the CAN-bus. The transferred torque is approximately proportional to the pressure in the clutch piston. The desired pressure can be achieved by choosing the corresponding stiffness value, which is then translated into a specific throttle valve position. [6]

2.2.2 Haldex Limited Slip Coupling Generation IV

The goal with the development of a fourth generation of the HLSC is to make a more cost efficient product. Since the number of sensors is closely related to the total cost, the pressure is no longer measured. This means that the pressure controller used in Generation II can not be used anymore.

The torque transfer between the front and the rear shaft is still caused by an oil pressure that controls the clutch piston forcing the discs in the multi-plate clutch together. The differences compared to Generation I lie in the way the pressurized oil is generated and how the pressure is controlled. In Generation IV the oil pressure is generated by a piston pump, run by an electric motor, and stored in an accumulator. This means that the pressurized oil is not automatically generated as soon as there is a differential wheel velocity, instead it is generated

in advance. In Generation IV the pressure is controlled by a proportional pressure valve. Compared to a throttle valve, the proportional pressure valve allows a more direct control of the pressure in the clutch piston and therefore also more direct control of the transferred torque. The pressure the valve produces inside the clutch piston will be an almost linear function of the control signal to the valve. [8]

2.3 Wheel and Vehicle Motion

For a vehicle with constant mass Newton's second law of motion can be applied to describe the motion in the longitudinal direction. In this simplified case the longitudinal force from the vehicle is counteracted only by the drag force and the gravitational force. The equation of motion then becomes

$$m\dot{v} = F_{tot} = F_x - F_d - mg\sin(\beta), \tag{2.2}$$

where m is the vehicle mass, v is the vehicle longitudinal velocity, F_x is the longitudinal force, F_d is the aerodynamic drag through the centre of gravity, g is the gravitational acceleration and β is the incline. The longitudinal force F_x is the sum of the driving or braking forces on the front and rear axles.[9]

The aerodynamic drag is calculated from

$$F_d = c_w A \frac{\rho}{2} v_x^{\,2}, \tag{2.3}$$

where c_w is the coefficient of wind resistance, A is the frontal area and ρ is the density of the air [10].

To calculate the angular velocity ω of the tyres a torque balance equation is defined for each tyre. The accelerating torque acting on each wheel comes from the driveline. The deceleration torque depends on the tyre friction and is calculated by the longitudinal wheel force multiplied by the radius of the tyre. Hence each tyre has the following rotational dynamic function

$$J_i \dot{\omega}_i = T_i - R_{ei} F_{xi}, \tag{2.4}$$

where J_i is the wheel tyre assembly inertia of rotation around spin axis, ω_i is the wheel angular velocity, T_i is the torque applied by the axle to the wheel and R_{ei} is the effective rolling radius. The effective rolling radius is not equal to static tyre radius, for further explanation se Section 2.4.1. To simplify the calculations a bicycle model is considered, i.e., a vehicle with one front and one rear wheel.

The sum of the torque applied by each axle to the wheels has to be equal to the total driving torque from the motor, i.e., [10]

$$T_{drive} = T_1 + T_2. \tag{2.5}$$

2.4 Wheel and Tyre Dynamics

Consider a wheel as in Figure 2.4 where v_x is the wheel centre longitudinal velocity, R is the tyre radius, ω is the wheel angular velocity and F_x is the longitudinal force.

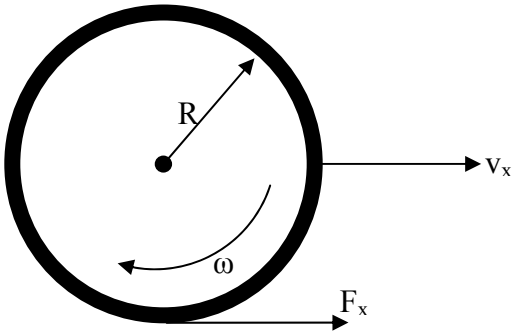

Figure 2.4 Typical wheel parameters.

2.4.1 Effective Rolling Radius

Figure 2.5 shows a tyre where R is the tyre radius for the undeflected tyre and R_l is the loaded radius, i.e., the wheel centre height above the road.

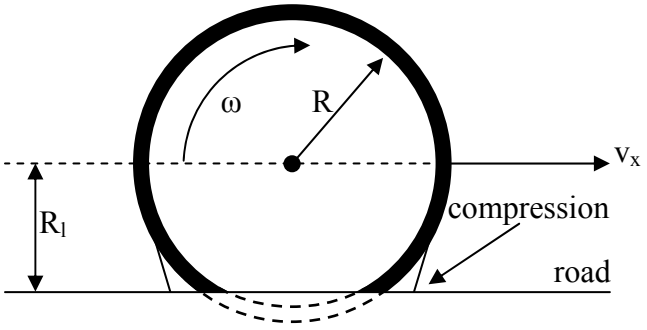

Figure 2.5 Tyre radius for the undeflected tyre and the loaded radius.

The effective rolling radius R_e is defined as the radius of the tyre when rolling without any external torque applied about the spin axis [9]. For a uniform, free rolling wheel the effective rolling radius is given by

$$R_e = \frac{v_x}{\omega_0}, \tag{2.6}$$

where ω_0 is the angular velocity at free rolling [11].

The effective rolling radius is the distance between the centre of rotation of the wheel body, called S, and the wheel spin axis. This distance depends on the tyre deflection ρ according to

$$R_e = R - f(\rho). \tag{2.7}$$

Since the tyre in reality is not completely uniform the undeflected tyre radius R may vary along the tyre circumference. The loaded radius equals the undeflected tyre radius minus the tyre deflection, i.e.,

$$R_l = R - \rho \,. \tag{2.8}$$

The effective radius depends on the tyre normal load F_z, the kind of tyre and the tread depth of the tyres. For a typical radial steel belted tyre the variations of the effective rolling radius behaves as in Figure 2.6. As can be seen in the figure the effective rolling radius can be approximated as constant for large tyre loads, which has be done in this project. [11]

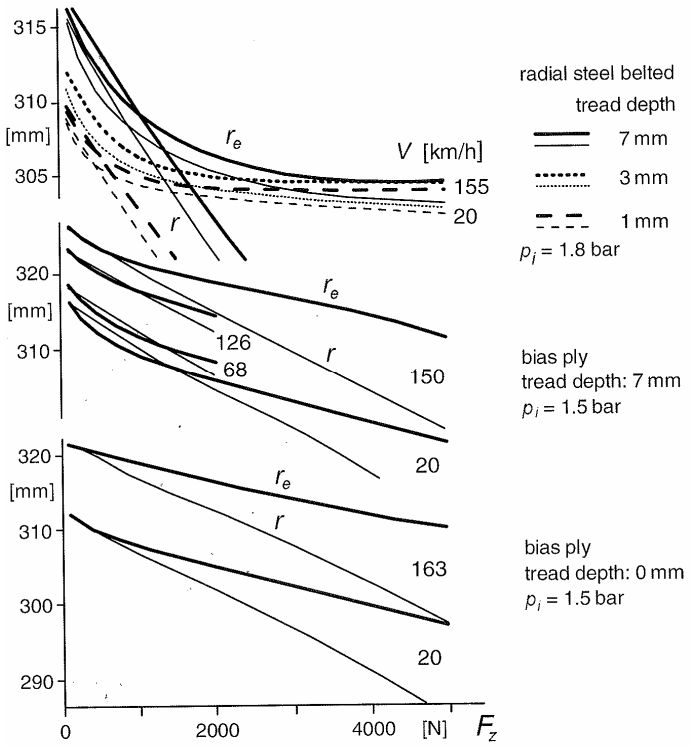

Figure 2.6 Tyre effective rolling radius and loaded radius as a function of tyre normal load at different speeds and for different tread depths and tyre design [11].

When the load is zero, S lies on the road surface or just below. The effective radius is then equal to the undeflected tyre radius. When a small tyre load is applied the point S may lie above the road. This is because the tread elements which come in contact with the road no longer have a radial direction but are vertically orientated. This results in that the rotation of these thread elements are lost which leads to a smaller effective radius. In this case the effective radius is equal to the radius R_c, see Figure 2.7. For a larger tyre load the point S will be located underneath the road surface. When a tyre has a ribbed tread pattern some rotation take place in the ribs in contact with the road. This enhances the effective radius and thus places the point S beneath the road level. [11]

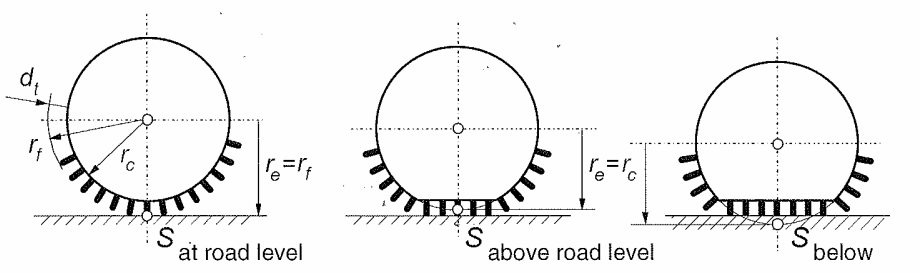

Figure 2.7 Location of the centre of rotation, the slip point S, at three different radial deflections [11].

2.4.2 Longitudinal Wheel Slip

The longitudinal wheel slip is defined as the difference between the angular velocity of the wheel and the longitudinal velocity of the vehicle acting through the centre of gravity. A difference occurs when a driving or braking force is applied to the tyres. There exist different ways to calculate the wheel slip, in this thesis the standard SAE definition is used [12]. A fictitious slip point S is defined as a point on the wheel rim with the distance R_e to the wheel centre and the velocity equal to zero at free rolling. When the longitudinal slip is not equal to zero, for example when the vehicle is driving or braking, the point S moves with the longitudinal slip velocity v_{sx} which is calculated through [11]

$$v_{sx} = v_x - \omega R_e . \tag{2.9}$$

The longitudinal wheel slip λ can now be defined as

$$\lambda = -\frac{v_{sx}}{v_x} = -\frac{v_x - \omega R_e}{v_x} = \frac{\omega R_e - v_x}{v_x}. \tag{2.10}$$

At perfect rolling the longitudinal slip will be zero, at driving, when $F_x > 0$, λ is positive and at braking, when $F_x < 0$, λ is negative. When the tyres are locked the angular velocity of the wheels is zero and the longitudinal slip will therefore be -1. [11]

2.4.3 Tyre Normal Load

The force acting perpendicularly to the surface at the wheel ground contact point is called the *tyre normal load* and is calculated from

$$F_z = mg\sin(\beta), \tag{2.11}$$

since the sum of the forces acting in the vertical direction has to be zero, in order for the vehicle not to elevate from the ground. The normal load is the sum of the load acting on the front and the rear wheel of the bicycle model. Generally the normal load is not evenly distributed between the wheel pairs since the vehicle typically weighs more at the front wheel pair. In this thesis the front tyre normal load is set to 60 % of the total load.

2.4.4 Longitudinal Force

The longitudinal tyre force is a function of the wheel slip at given values of normal force, road surface conditions, tyre characteristics etc. The typical behaviour of the curve can be seen in Figure 2.8. The longitudinal force starts with a steep rise due to elastic deformation of the tread. This behaviour can approximately be described by the linear function

$$F_x = C_x \lambda \,, \tag{2.12}$$

where C_x is the effective longitudinal stiffness of the tyre. The value of C_x depends on the construction of the tyre and on inflation pressure. As the longitudinal slip increases the tread elements at the contact surface with the road will eventually reach its limit of distortion and start to slip. The slope of the curve thus decreases until the longitudinal force reaches its peak. The amplitude of the peak depends on the friction between the tyre and the road surface. The larger the friction is the larger the maximum force will be. Beyond the peak, the tyre force decreases and the tyre slip dynamics will get unstable, and after a while it approaches a horizontal asymptote. [9]

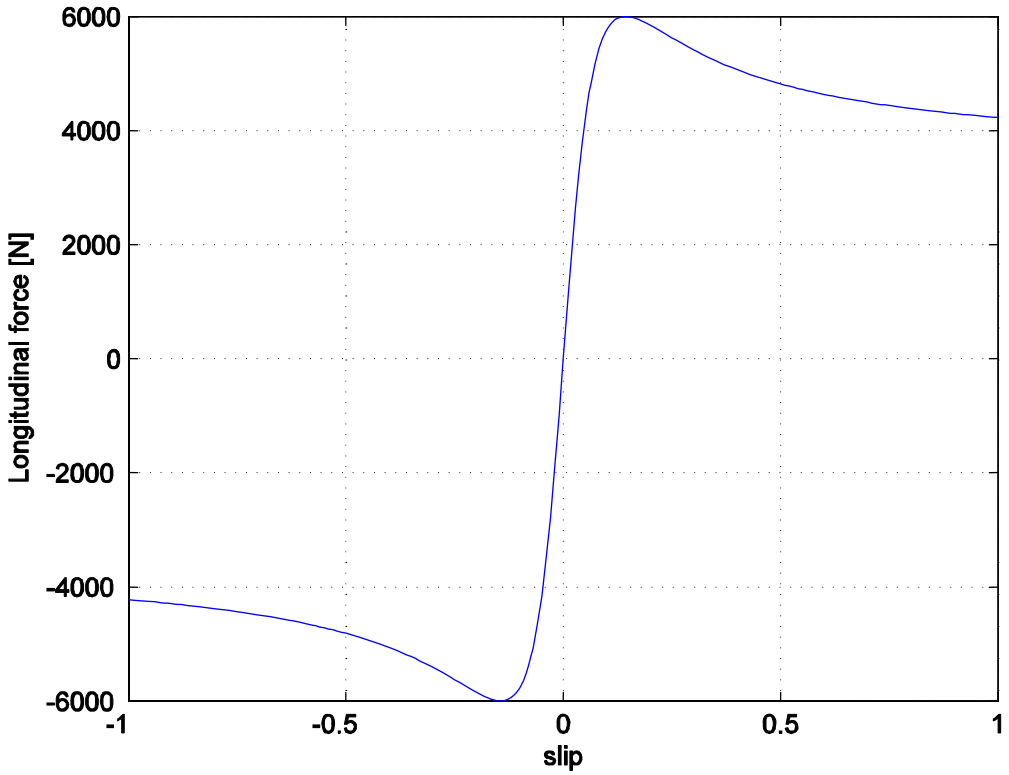

Figure 2.8 Longitudinal force F_x as a function of the longitudinal slip λ for a typical tyre.

To approximate the behaviour of the longitudinal force with respect to slip Pacejka's *Magic Formula* can be used. This method fits measurement data to the force curve. For pure longitudinal slip the formula reads

$$F_x = D\sin\left(C\arctan\left(B\lambda - E\left(B\lambda - \arctan\left(B\lambda\right)\right)\right)\right) \tag{2.13}$$

where B is the stiffness factor, C is the shape factor, D is the peak value and E is the curvature factor. The parameters are shown in Figure 2.9. The formula generates a curve which passes through the origin with the angle $\arctan\left(B \cdot C \cdot D\right)$, rises to the maximum force D at the slip x_m and finally decreases and approaches a horizontal asymptote y_a. [11]

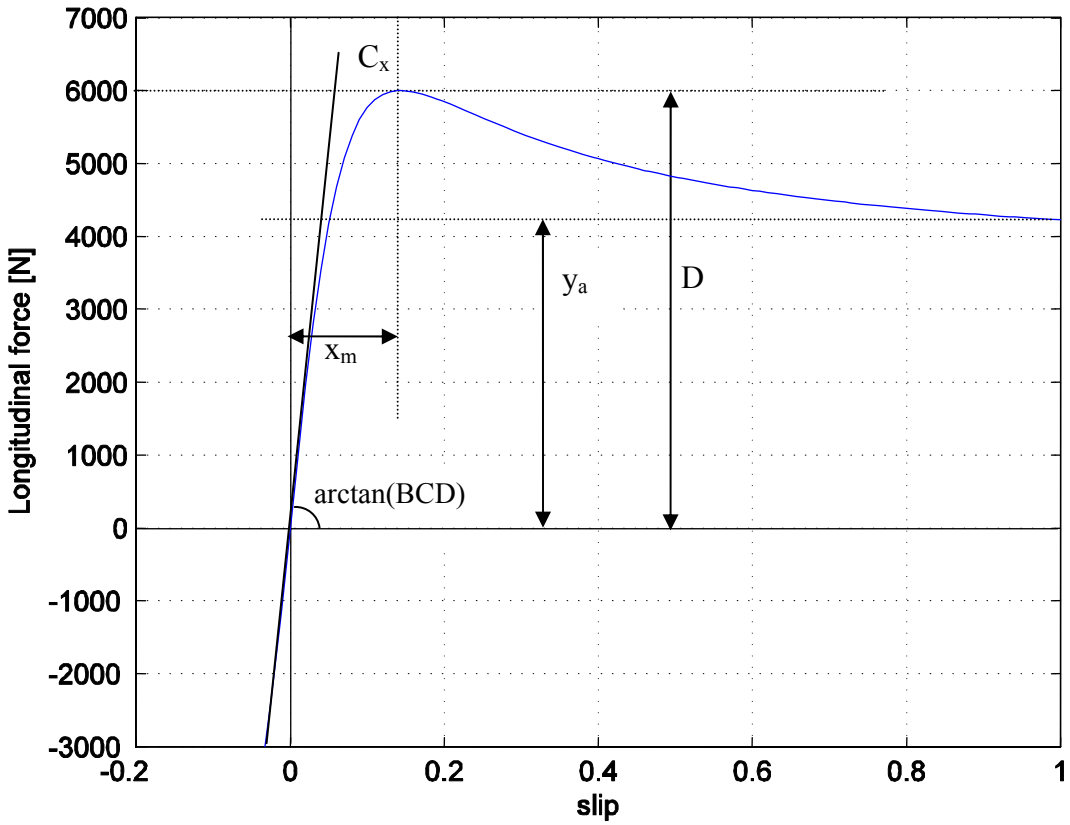

Figure 2.9 Longitudinal force F_x as a function of the longitudinal slip λ with curve parameters.

Since the force can be described by Equation (2.12) for λ close to zero it can be shown that

$$C_x = B \cdot C \cdot D \,. \tag{2.14}$$

The value of the coefficient C is chosen depending on the type of directional force that is acting on the tyres, e.g., braking force or lateral force. The peak value D can be calculated through

$$D = \mu F_z \tag{2.15}$$

where μ is the friction between the tyre and the road surface and F_z is the tyre normal load which is defined by Equation (2.11). If the value of the effective longitudinal stiffness C_x is known B can be calculated according to Equation (2.14).

The asymptote y_a is determined by

$$y_a = D \sin\left(\frac{\pi}{2} C\right). \tag{2.16}$$

It can be shown that the curvature factor E can be calculated from

$$E = \frac{Bx_m - \tan\left(\frac{\pi}{2C}\right)}{Bx_m - \arctan\left(Bx_m\right)} \tag{2.17}$$

where x_m is the slip where the force has reached its maximum value, as shown in Figure 2.9.

For simplicity the value of the coefficient E is set to zero in this thesis which gives

$$x_m = \frac{1}{B}\tan\left(\frac{\pi}{2C}\right). \tag{2.18}$$

The curve shown in Figure 2.8 is generated through the Magic Formula with the coefficients $C_x = 1 \cdot 10^5$, $C = 1.6$, $D = 6000$ and $E = 0$. [13]

3 Modelling and Control

The chapter starts with a presentation of the method used when designing the control system in the thesis. This method is the basis of the structure of the chapter. This includes one section where the specifications on the controllers are presented, one where the models used in the simulations are explained, one where the design of the controller is outlined and one section about the simulations and how they were evaluated. At last some comments on the implementation of the control system are found.

3.1 Course of Action

When designing a controller the following general approach with five basic steps presented in [14] was used.

1) Specify desired behaviour of the controller and choose actuators and sensors.
For linear systems quantitative specifications are often identified for the controller but this is usually not possible for nonlinear systems. Instead a number of qualitative specifications in the operating range of the controller are considered. Following issues are important to take into consideration:

- Stability
- Accuracy and speed of response
- Robustness
- Cost

A control system typically has to compromise between the four dimensions.

2) Model the physical system with a set of differential equations
It is important that the model is easy to understand and handle but still accurate enough. More accurate models are not necessarily better since they may require more complex controllers than actually needed. The model should also give a feeling of the model uncertainties that exist due to divergence between the real system and the model.

3) Design a controller for the system
There is no general method for designing nonlinear controllers. Instead there exis many different and complementing methods that are suited for different nonlinear problems. In the same way as when designing linear controls systems, feedback is important. However, for nonlinear systems feed forward also plays an important part.

4) Analyse and simulate the control system
An efficient way to ensure that the specifications are met is to simulate the system.

5) Implement the control system in the hardware

3.2 Specifications

When controlling a physical system it is important to understand what the main goals for the control are. Two common requirements on a controller are set point following and disturbance elimination. There are a number of limitations that make it difficult to control a system from the specifications, e.g., system dynamics, nonlinearities, disturbances and process

uncertainties. It is important to have clear specifications on a system before starting to control it. Typical specifications are

- Moderation of load disturbances
- Sensitivity to measurement noise
- Robustness to model uncertainty
- Set point following.

Load disturbances force the output signal away from the desired trajectory which gives an error *e(t)*. There exists many different ways of quantifying the error such as the maximum error e_{max} and the settling time t_s, defined as the time it takes for the error to become smaller than $\pm p$, where p is often set to 5 %. A further common method used in this thesis is the integrated absolute error [15]

$$IAE = \int_0^\infty |e(t)|\,dt = \int_0^\infty |y(t) - y_{sp}(t)|\,dt\,. \tag{3.1}$$

The set point signal, i.e., the desired value for the difference between the velocity of the front and rear wheel pair, is small but increases with the vehicle velocity and can be chosen as a percentage of the longitudinal velocity of the vehicle, in this thesis 2 % was chosen.

The specifications of the slip controller have to be a compromise between a fast and a slow controller. A fast controller makes the vehicle safe because it counteracts a slip fast. A slow controller however is less affected by the noise in the system and does not have a jerky performance which would affect the driving comfort in the car in a negative sense.

Since the task is to compare the performance of the two slip controllers in Generation I and Generation IV to each other no specifications where set in advance. Instead the performance where evaluated with respect to possible specifications for the two different control systems.

3.3 Modelling

The two models for slip control in Generation I and Generation IV look alike on a high level, they both contain the same blocks; a controller, the HLSC, a torque transfer model and a vehicle model, see Figure 3.1. There is also a load disturbance, T_{drive}, which occurs when the driver steps on the gas. The CAN-bus is modelled as a time delay on the measurement signal, *y*.

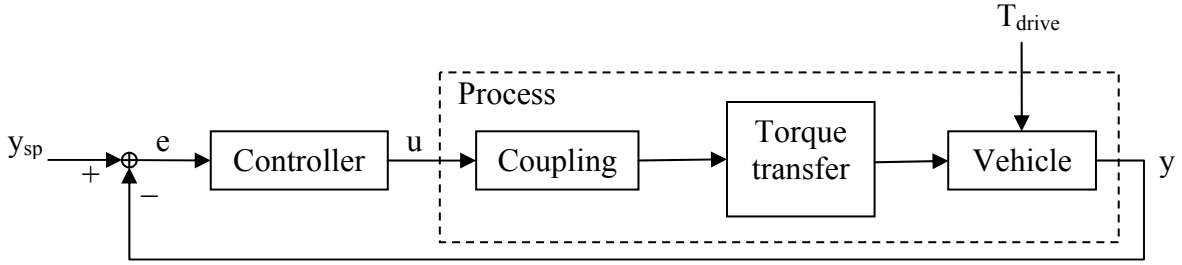

Figure 3.1 Basic structure of the modelled system.

The models are made in Matlab's simulation tool Simulink, see [16] for more information. In this section the separate blocks in the model are explained individually. The Matlab/Simulink programs for the two models are shown in Appendix C.

3.3.1 Vehicle Model

The vehicle model is a simple driveline model as can be seen in Figure 3.2. The engine is represented by the driveline torque, T_{drive}. The model is a bicycle model of a vehicle driving straight ahead.

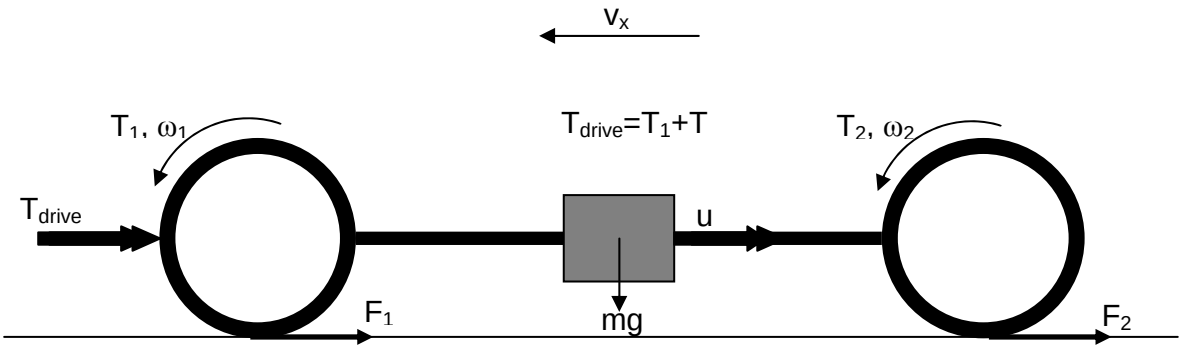

Figure 3.2 The simple driveline model used as a basis for the simulations.

To get reliable results from the simulations the vehicle parameters in the model has to have realistic values. A Volvo S 40 with AWD was used as a reference car for the choice of parameter values such as weight and wheelbase in the thesis. [17]

When the Simulink math operation *Divide* is used a division through zero has to be avoided. The signal in the denominator is thus filtered through the subsystem *No Division by Zero*. The main idea is to detect when the input signal approaches zero and then add a small number to ensure that the signal never becomes equal to zero. As a small number the value *eps* is used, this is a predefined number in Matlab with the value $2.2204 \cdot 10^{-16}$. As an input signal u the output signal y is accordingly

$$y = u + \sigma \tag{3.2}$$

where

$$\sigma = \begin{cases} 0 & for\ |u| \geq eps \\ (+1) \cdot eps & for\ 0 \leq u < eps \\ (-1) \cdot eps & for\ 0 > u > -eps. \end{cases} \tag{3.3}$$

The Matlab/Simulink program for the "*no division by zero*"-model is shown in Appendix C.3.2.

The vehicle model is divided into three subsystems, the vehicle body, the wheels and the tyres. Each subsystem is explained below.

Vehicle Body

The subsystem *vehicle body* calculates the longitudinal velocity v_x of the vehicle from Equations (2.2) and (2.3). The input signal is the longitudinal force, which is the sum of the longitudinal forces F_1 and F_2 acting on the front and rear tyres respectively. The Matlab/Simulink program for the vehicle body is shown in Appendix C.3.3.

Wheels

From Equations (2.4) and (2.5) the angular velocities ω_1 and ω_2 of the front and rear wheels are derived in the subsystem *wheels*. The input signal T_{drive} is the driveline torque and can be viewed as the load disturbance. The signal T_2 is obtained from the *torque transfer model* described in Section 3.3.2. The Matlab/Simulink program for the wheels is shown in Appendix C.3.4.

Tyres

The longitudinal forces F_1 and F_2 acting on the front and rear tyres are calculated in the subsystem *tyres* with Equations (2.10) and (2.13). Its input signals are the output signals from the two other subsystems in the vehicle model and its output signals are the input signals in the subsystem *wheels*. The subsystem *no division by zero* is used, for explanation see Section 3.3.1. The Matlab/Simulink program for the tyres is shown in Appendix C.3.5.

3.3.2 Torque Transfer Model

The actual torque transfer has to be calculated from the torque capacity, which is the signal being controlled, and the difference between the angular velocity of the front and rear shafts $\Delta\omega$. For large angular velocity the actual torque transferred is limited to the torque capacity due to the stiffness of the multi-plate clutch. The behaviour is illustrated in Figure 3.3.

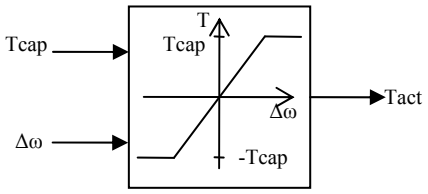

Figure 3.3 Torque transfer model.

In the simulations this behaviour was modelled using the hyperbolic tangent function defined as

$$\tanh(dx) = \frac{\sinh(dx)}{\cosh(dx)} = \frac{e^{dx} - e^{-dx}}{e^{dx} + e^{-dx}}. \qquad \textbf{(3.4)}$$

To get a steeper inclination the factor d can be increased, in the simulations $d = 5$ is used. The output value, which depends on the difference between the front and the rear shaft rotational velocity $\Delta\omega$, is then multiplied with T_{cap} from the coupling to get the value of the actual transferred torque. The Matlab/Simulink program for the torque transfer model is shown in Appendix C.4.

3.3.3 Coupling

The coupling calculates the desired torque to be transferred to the rear shaft depending on the output from the controller. Since the hardware in the coupling is significantly different in the two generations considered, the models are discussed separately below.

HLSC Generation I

In HLSC Generation I the slip is controlled both directly by the slip controller and indirectly by a differential pump that counteracts a difference between the velocity of the front and rear

shaft, see Section 2.2 for more details. The differential pump generates a pump flow which is approximately proportional to the differential angular velocity.

The calculated torque to be applied to the rear shaft is thus dependent on both the control output u and the differential angular velocity $\Delta\omega$ and can be approximately modelled by

$$\dot{T} = c\left(\Delta\omega - \frac{T}{u}\right) \tag{3.5}$$

where c is a constant describing the hydraulic mechanical stiffness of the coupling. The Matlab/Simulink program for the coupling in HLSC Generation I is shown in Appendix C.5.1.

HLSC Generation IV

In HLSC Generation IV the torque which should be transferred to the rear shaft in order to even the angular velocity of the shafts, is controlled directly by the controller. An extra computation of the desired torque is hence not necessary. The coupling is instead modelled by a transfer function with a time constant τ which represents the time it takes for the discs in the multi-plate clutch to be forced together, see to Section 2.2 for more details. The output torque from the coupling will be

$$T = \frac{1}{s\tau + 1}u\,. \tag{3.6}$$

The Matlab/Simulink program for the coupling in HLSC Generation IV is shown in Appendix C.5.2.

3.4 Control

When designing a slip controller, difficulties occur due to the high nonlinearity of the tyre characteristics. Hence as a first step a linearization of the vehicle model was made. A further difficulty is the time delay from the CAN-bus. A modified PID controller was used. Different design methods where tested to attempt to find a suitable control law for the two systems.

3.4.1 Linearization of the Vehicle Model

The vehicle model can be described through the Equations (2.2) - (2.4) which gives the following state equations

$$\dot{\omega}_1 = \frac{1}{J_1}\left(T_1 - R_{e1}F_{x1}\right) \tag{3.7}$$

$$\dot{\omega}_2 = \frac{1}{J_2}\left(T_2 - R_{e2}F_{x2}\right) \tag{3.8}$$

$$\dot{v} = \frac{1}{m}\left(F_{x1} + F_{x2} - F_d - mg\sin(\beta)\right). \tag{3.9}$$

If the velocity of the vehicle is viewed as constant for a small time period, the derivative of the velocity will be equal to zero, which eliminates Equation (3.9). The state equations will be nonlinear since the longitudinal force F_{xi} is a function of the slip calculated by Pacejka's nonlinear Magic Formula, Equation (2.13). The slip, as defined in Equation (2.10), is a

function of the velocity v and the angular velocity ω of the wheel. Since the velocity is viewed as constant for a small time period the slip simplifies as a function of ω. The longitudinal force can thus be expressed as

$$F_{xi} = f_i(\lambda_i) = f_i(\lambda_i(\omega_i)) = g_i(\omega_i). \tag{3.10}$$

The state equations in Equations (3.7) and (3.8) together with Equation (2.5) can therefore be written as a nonlinear system according to

$$\begin{aligned} \dot{\boldsymbol{\omega}} &= \begin{pmatrix} -\frac{R_{e1}}{J_1} g_1(\omega_1) \\ -\frac{R_{e2}}{J_2} g_2(\omega_2) \end{pmatrix} + \begin{pmatrix} -\frac{1}{J_1} \\ \frac{1}{J_2} \end{pmatrix} T_2 + \begin{pmatrix} \frac{1}{J_1} \\ 0 \end{pmatrix} T_{drive} \\ y &= \begin{pmatrix} R_{e1} & -R_{e2} \end{pmatrix} \boldsymbol{\omega} \end{aligned} \tag{3.11}$$

where $\boldsymbol{\omega}$ can be viewed as the state vector, T_2 as the control signal and T_{drive} as a load disturbance. The process signal y is the differential longitudinal velocity of the tyres, Δv, measured in ms^{-1}.

A linearization of the vehicle model can be performed by using Taylor series which is a way of expanding a function about a point x_0 [18]

$$f(x) = f(x_0) + \frac{\partial}{\partial x} f(x)\Big|_{x_0} (x - x_0) + \frac{\partial^2}{\partial x^2} f(x)\Big|_{x_0} \frac{(x - x_0)^2}{2!} + \sigma^3(f(x)). \tag{3.12}$$

The linearization point in this case is $(\omega_1^0, \omega_2^0, T_{drive}^0, T_2^0)$, where T_{drive}^0 and T_2^0 are chosen so that

$$\dot{\omega}_1(\omega_1^0, \omega_2^0, T_{drive}^0, T_2^0) = \dot{\omega}_2(\omega_1^0, \omega_2^0, T_{drive}^0, T_2^0) = 0. \tag{3.13}$$

This gives

$$0 = -\frac{R_{e1}}{J_1} g_1(\omega_1^0) + \frac{1}{J_1} T_{drive}^0 - \frac{1}{J_1} T_2^0 \Rightarrow T_{drive}^0 = R_{e1} g_1(\omega_1^0) + T_2^0 \tag{3.14}$$

$$0 = -\frac{R_{e2}}{J_2} g_2(\omega_2^0) + \frac{1}{J_2} T_2^0 \Rightarrow T_2^0 = R_{e2} g_2(\omega_2^0). \tag{3.15}$$

Applying Taylor expansion on the state equations from Equation (3.11) gives the linear expression

$$\begin{aligned} \dot{\omega}_1 &\approx -\frac{R_{e1}}{J_1} \left(g_1(\omega_1^0) + \frac{\partial g_1}{\partial \omega_1}\Big|_{\omega_1 = \omega_1^0} (\omega_1 - \omega_1^0) \right) + \frac{1}{J_1} T_{drive}^0 - \frac{1}{J_1} T_2^0 \\ \dot{\omega}_2 &\approx -\frac{R_{e2}}{J_2} \left(g_2(\omega_2^0) + \frac{\partial g_2}{\partial \omega_2}\Big|_{\omega_2 = \omega_2^0} (\omega_2 - \omega_2^0) \right) + \frac{1}{J_2} T_2^0. \end{aligned} \tag{3.16}$$

Together with Equations (3.14) and (3.15) each state equation can be simplified as follows

$$\begin{aligned}\dot{\omega}_1 &= -\frac{R_{e1}}{J_1}\frac{\partial g_1}{\partial \omega_1}\bigg|_{\omega_1=\omega_1^0}\left(\omega_1-\omega_1^0\right)-\frac{R_{e1}}{J_1}g_1\left(\omega_1^0\right)+\frac{1}{J_1}T_{drive}^0-\frac{1}{J_1}T_2^0\\ &= -\frac{R_{e1}}{J_1}\frac{\partial g_1}{\partial \omega_1}\bigg|_{\omega_1=\omega_1^0}\left(\omega_1-\omega_1^0\right)-\frac{R_{e1}}{J_1}g_1\left(\omega_1^0\right)+\frac{1}{J_1}R_{e1}g_1\left(\omega_1^0\right)+\frac{1}{J_1}T_2^0-\frac{1}{J_1}T_2^0\\ &= -\frac{R_{e1}}{J_1}\frac{\partial g_1}{\partial \omega_1}\bigg|_{\omega_1=\omega_1^0}\left(\omega_1-\omega_1^0\right)\end{aligned} \tag{3.17}$$

and

$$\begin{aligned}\dot{\omega}_2 &= -\frac{R_{e2}}{J_2}\frac{\partial g_2}{\partial \omega_2}\bigg|_{\omega_2=\omega_2^0}\left(\omega_2-\omega_2^0\right)-\frac{R_{e2}}{J_2}g_2\left(\omega_2^0\right)+\frac{1}{J_2}T_2^0\\ &= -\frac{R_{e2}}{J_2}\frac{\partial g_2}{\partial \omega_2}\bigg|_{\omega_2=\omega_2^0}\left(\omega_2-\omega_2^0\right)-\frac{R_{e2}}{J_2}g_2\left(\omega_2^0\right)+\frac{1}{J_2}R_{e2}g_2\left(\omega_2^0\right)\\ &= -\frac{R_{e2}}{J_2}\frac{\partial g_2}{\partial \omega_2}\bigg|_{\omega_2=\omega_2^0}\left(\omega_2-\omega_2^0\right).\end{aligned} \tag{3.18}$$

Let

$$\begin{aligned}z_1 &= \omega_1-\omega_1^0 \Rightarrow \dot{z}_1=\dot{\omega}_1\\ z_2 &= \omega_2-\omega_2^0 \Rightarrow \dot{z}_2=\dot{\omega}_2.\end{aligned} \tag{3.19}$$

The linearized and transformed system hence has the eigenvalues

$$\begin{aligned}\nu_1 &= -\frac{R_{e1}}{J_1}\frac{\partial g_1}{\partial \omega_1}\bigg|_{\omega_1=\omega_1^0}=-\frac{R_{e1}}{J_1}\frac{B_1CD_1R_{e1}\cos\left(C\arctan\left(\frac{B_1\left(R_{e1}\omega_1^0-v\right)}{v}\right)\right)}{v\left(1+\frac{B_1^2\left(R_{e1}\omega_1^0-v\right)^2}{v^2}\right)}\\ \nu_2 &= -\frac{R_{e2}}{J_2}\frac{\partial g_2}{\partial \omega_2}\bigg|_{\omega_2=\omega_2^0}=-\frac{R_{e2}}{J_2}\frac{B_2CD_2R_{e2}\cos\left(C\arctan\left(\frac{B_2\left(R_{e2}\omega_2^0-v\right)}{v}\right)\right)}{v\left(1+\frac{B_2^2\left(R_{e2}\omega_2^0-v\right)^2}{v^2}\right)}.\end{aligned} \tag{3.20}$$

The goal is to determine how the vehicle velocity affects the possibility to bring the system back to the set point signal after it has been disturbed. If the vehicle is driven with a velocity v the controlled process signal $y = v_1\text{-}v_2 = 0.02 \cdot v$.

The linearization was performed along a trajectory where $0 \leq \lambda_1^0 \leq 0.4$ to ensure that the transition between the linear and the nonlinear region is covered. This means that the vehicle model is linearized for

$$\frac{v}{R_{ei}}(1+0) \leq \omega_i^0 \leq \frac{v}{R_{ei}}(1+0.4) \Leftrightarrow \frac{v}{R_{ei}} \leq \omega_i^0 \leq \frac{v}{R_{ei}} 1.4. \tag{3.21}$$

To get a feeling for how the system reacts to different vehicle velocities the eigenvalues where plotted for one low velocity, $v = 5$ ms^{-1}, and for one faster velocity, $v = 20$ ms^{-1}. The results can be seen in Figure 3.4 and Figure 3.5.

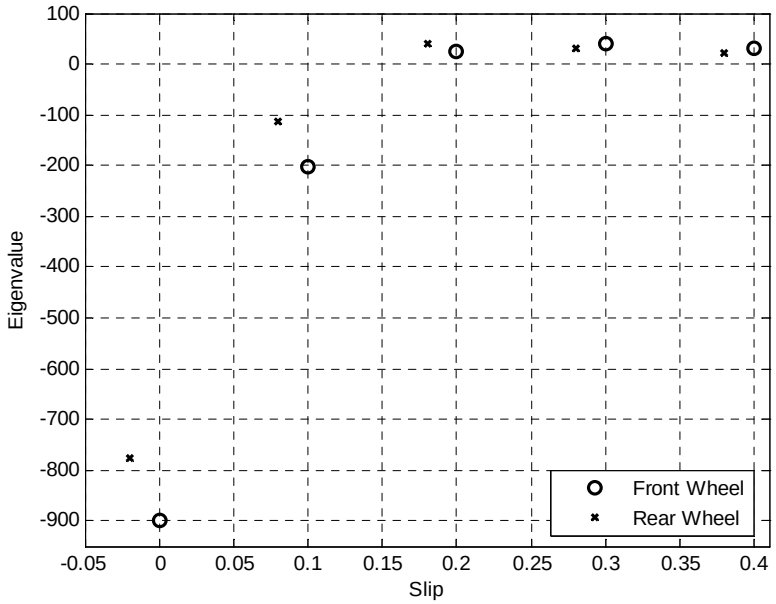

Figure 3.4 The eigenvalues of the vehicle model for v=5 ms^{-1}.

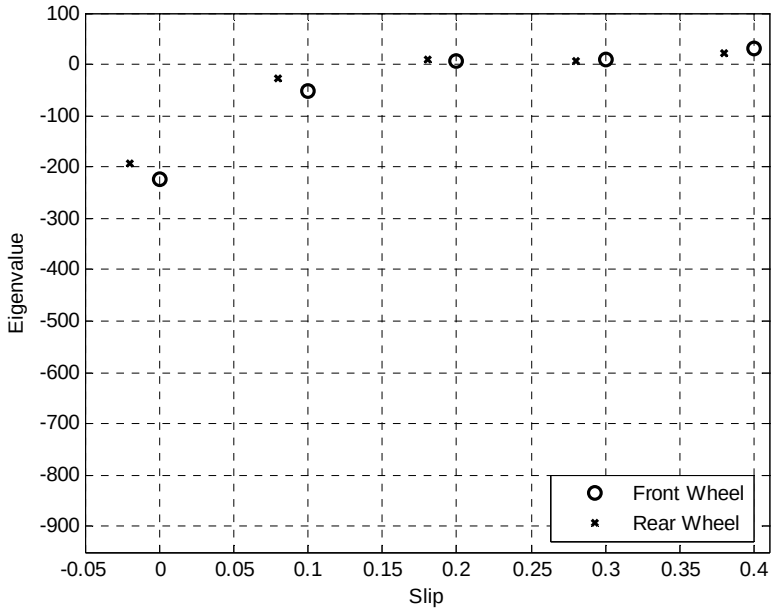

Figure 3.5 The eigenvalues of the vehicle model for v=20 ms^{-1}.

The figures show that for small slip, i.e., the linear region, the eigenvalues will have a more negative real part, which means that the system will be more stable for small velocities. This is however not the most interesting region from a control design perspective. Instead focus should be just above the peak where the slip must be controlled back to the peak value as fast as possible. Here the eigenvalues has a positive real part for both velocities which agrees with the discussion about Pacejka's Magic Formula in Section 2.4.4. It can however be seen that for low velocities the real parts of the eigenvalues are larger than for large velocities which implies that the slip should be easier to control for large velocities. This suggests that it might be advantageous to change the control parameters with the vehicle velocity.

3.4.2 Digital PID Controllers

The general equation of a time continuous PID controller is

$$u(t) = K\left(e(t) + \frac{1}{\tau_i}\int_0^t e(s)ds + \tau_d \frac{de(t)}{t} \right) \tag{3.22}$$

where e(t) is the error according to

$$e(t) = y_{sp}(t) - y(t). \tag{3.23}$$

When implementing a PID controller on time discrete form there may be benefits from altering the equation to fit the current situation. One important issue to be considered is that a pure derivative can not and should not be implemented since it gives a large amplification of the measurement noise. The derivative gain can be limited through the approximation

$$s\tau_d \approx \frac{s\tau_d}{1 + \frac{s\tau_d}{N}}. \tag{3.24}$$

The approximation works well for low frequencies but the gain is limited to N for high frequencies which may not always be advantageous. The value of N is usually chosen somewhere between 3 and 20. Two further changes made to the equation of the PID controller in this report are presented below. [19]

Integrator Windup

The control signal which can actually be carried out by an actuator is limited for most physical systems. This can result in a control signal saturation which, if a controller with an integrator is used, can lead to an effect called *integrator windup*. When the control error becomes large the integrator will saturate the actuator and it will stay saturated even if the process output signal is changed. The integrator can then integrate up to a large value and become so large that it takes a long time before it regains a normal value after the error has decreased. In the mean time the control signal will stay at its maximum value. Integrator windup typically occurs when there is a large set point change or at large disturbances or equipment failures. [20]

There are several possibilities to prevent integrator windup. One is to stop updating the integral when the actuator is saturated. Another way is with tracking. An error signal e_s is then calculated as the difference between the actuator output u and the controller output u_c, and fed

back to the integrator through the gain $1/\tau_t$, see Figure 3.6. The error is zero when the actuator is not saturated. When the actuator on the other hand becomes saturated, the feedback loop will reset the integrator, keeping the controller output signal at the limit of saturation by struggling to keep the error as close to zero as possible. The integrator is thus reset to an appropriate value dynamically with the tracking time constant τ_t. The smaller time constant chosen, the faster the integrator is reset. It may be tempting to always choose a very small τ_t, for systems with a derivative part this is however not always advantageous since false errors may cause the output to saturate, which by mistake resets the integral. The tracking time constant, τ_t, should be larger than τ_d and smaller than τ_i.

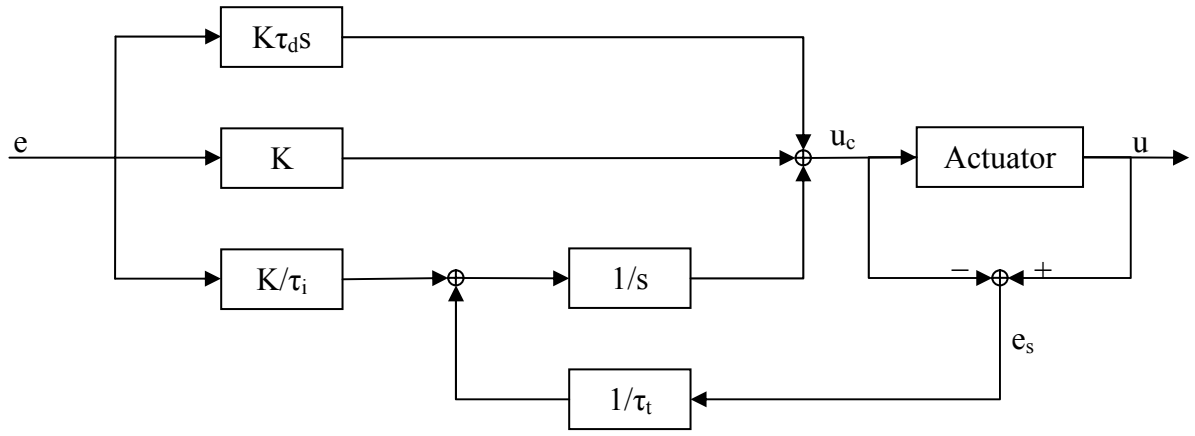

Figure 3.6 Controller with anti-windup [19].

The main advantage of this method is that it can be applied to all kinds of actuators, e.g., saturation, dead zone and hysteresis, as long as the actuator output signal is measurable. [19]

Set Point Weighting

Usually the error is calculated through the difference between the set point signal and the output signal from the process. The error is then the input signal to the controller. A better result can often be received if the set point and the process output are treated separately in the controller. This can be done with so called set point weighting, which gives the following PID controller

$$u(t) = K\left(e_p + \frac{1}{T_i}\int_0^t e(s)ds + T_d \frac{de_d}{dt} \right) \tag{3.25}$$

where the error in the proportional part is

$$e_p = ay_{sp} - y \tag{3.26}$$

and the error in the derivative part is

$$e_d = by_{sp} - y\,. \tag{3.27}$$

The error in the integral part is the true error

$$e = y_{sp} - y \tag{3.28}$$

so that steady-state control errors are avoided.

How the controller reacts on load disturbances and measurement noise does not depend on the values of *a* and *b*. Different values on *a* and *b* does however give different response to set point changes. The smaller value of *a*, the smaller the overshoot caused by a change in the set point will be. To avoid large transients in the control signal when the set point changes sudden, the parameter *b* is usually set to zero. [15]

The controller in Equations (3.25) - (3.28) gives the system in Figure 3.7.

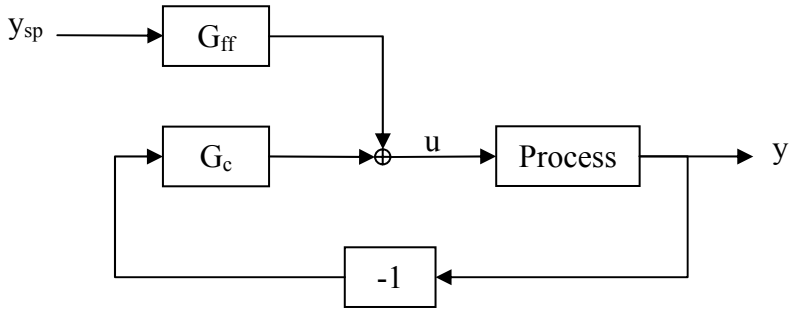

Figure 3.7 Block diagram of a system with set point weighting [15].

The transfer functions for the system with set point weighting are thus [15]

$$G_{ff}(s) = K\left(a + \frac{1}{s\tau_i} + bs\tau_d\right) \tag{3.29}$$

$$G_c(s) = K\left(1 + \frac{1}{s\tau_i} + s\tau_d\right). \tag{3.30}$$

3.4.2.1 Modified PID Controller

After the above suggested modifications the original PID controller in Equation (3.22) will instead have the transfer function

$$U_c(s) \approx K\left(\left(a + \frac{1}{s\tau_i} + b\frac{s\tau_d}{1+\frac{s\tau_d}{N}}\right)Y_{sp}(s) - \left(1 + \frac{1}{s\tau_i} + \frac{s\tau_d}{1+\frac{s\tau_d}{N}}\right)Y(s)\right) + \frac{1}{s\tau_t}\left(U(s) - U_c(s)\right) \tag{3.31}$$

according to earlier introduced notations. This is the transfer function used in the simulations.

3.4.3 Tuning Maps

Tuning methods only give an approximate idea of how to tune the parameters of the controller. Further adjustments need to be done in order to find the optimal parameter settings. A systematic way to do this is to use so called tuning maps. Two parameters are changed one at a time and the performance of the control system is evaluated through, e.g., frequency responses. The result is then arranged in a matrix to give a feeling for how changes of control

parameters affect the performance of the system. On example of a tuning map is the tuning of a PID controller for the process with the transfer function $G(s) = (s+1)^{-8}$ which can be seen in Figure 3.8. [15]

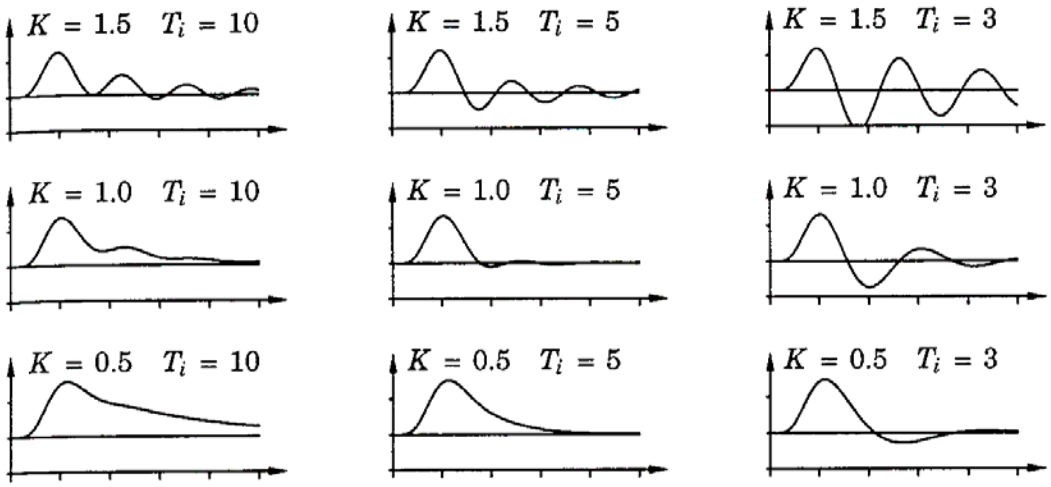

Figure 3.8 Tuning map for PID control of a process with the transfer function $G(s) = (s+1)^{-8}$. The responses for different values on K and τ_i to a unit step disturbance at the process input are plotted for $\tau_d = 1.9$ [15].

One drawback with the method is that in order to analyze the affects of all three control parameters in a PID controller at one time a three dimensional array would be needed and the advantage of overview would be lost.

Rules of thumb that can be used when manually tuning the controller parameters of a PID controller are shown in Table 3.1. The table shows how changes on the parameters K, τ_i and τ_d affect the speed and the stability of the control loop. One other problem with the rules are that they only tell whether the parameters should be increased or decreased but the difficulty is often to know how much they should be adjusted. [15]

Table 3.1 Rules of thumb for the effects of the controller parameters on speed and stability [15].

		Speed	Stability
K	+	+	−
τ_i	+	−	+
τ_d	+	+	+

3.4.4 Gain Scheduling

Gain Scheduling is a method for nonlinear processes, time variant processes and processes where the control changes with the operating conditions. The main idea is to divide the total operating range into smaller areas where the system is approximately linear. A measurable variable that change with the different operating conditions is chosen, e.g., the measurement signal, the control signal or an extern signal. For the chosen variable limits where the system enters a new operating range are defined. The different operating ranges are then analyzed and control parameters for each area are determined. Figure 3.9 shows the basic block diagram for a system with gain scheduling.

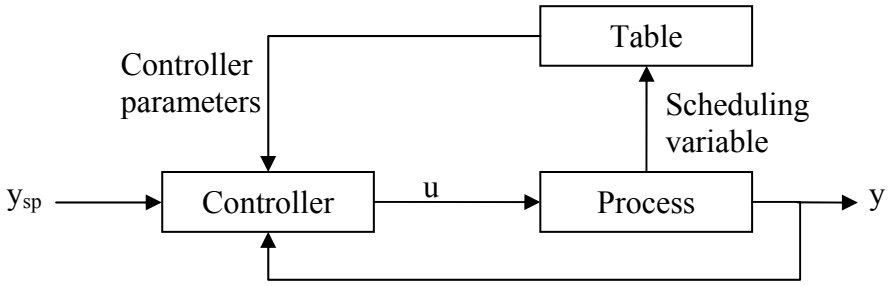

Figure 3.9 Block diagram of a system with gain scheduling [15].

The method has the advantage of following fast changes in the operating conditions and often only a few different parameter sets are necessary to accomplish this. Problems can however occur when the changes in the operating conditions are too frequent. The scheduling has to be significantly slower than these changes. The basic procedure of the method can be summarized in four steps: [15]

1) Choose a measurable variable for the scheduling

2) Find limits for the variable in the different operating ranges

3) Determine controller parameters in the different operating ranges

4) Store the limits and the parameters in a table

Since the stability of the system is highly dependable of the vehicle velocity this appears to be a suitable choice of variable for the gain scheduling. The vehicle velocity is however not a measurable variable but the wheel velocity is available on the CAN-bus. It is thus possible to convert the angular velocity into longitudinal velocity by multiplying with a predefined value for the wheel radius. This will not always give a completely correct value of the vehicle velocity but constitutes a sufficient approximation.

3.4.5 Tuning

When tuning the slip controller the vehicle was considered driving uphill with a constant driveline torque. The velocity was first set to 20 ms^{-1} and then to 5 ms^{-1}. Since the effective rolling radius is not identical for the front and the rear wheel there will be a small difference between the angular wheel velocities. This can be viewed as a step in the set point signal at time $t=0$. The time it takes for the system to settle this step response should be minimized with well tuned control parameters.

To get a feeling of the magnitude of the control parameters, tuning maps were used. When approximate values of the parameters were determined further investigation was made by comparing the settling time for different combinations. The parameter tuning was done separately for the slip controller in Generation I and Generation IV and the working procedures are described below.

Generation I

To get a first estimation of the suitable parameter settings in Generation I a tuning map over a wide range of parameter combinations were plotted. Figure 3.10. shows an example of a tuning map with the parameter values $K = -10, -20, -30$ [Ns^2] and $\tau_i = 0.001, 0.01, 0.1$ [s].

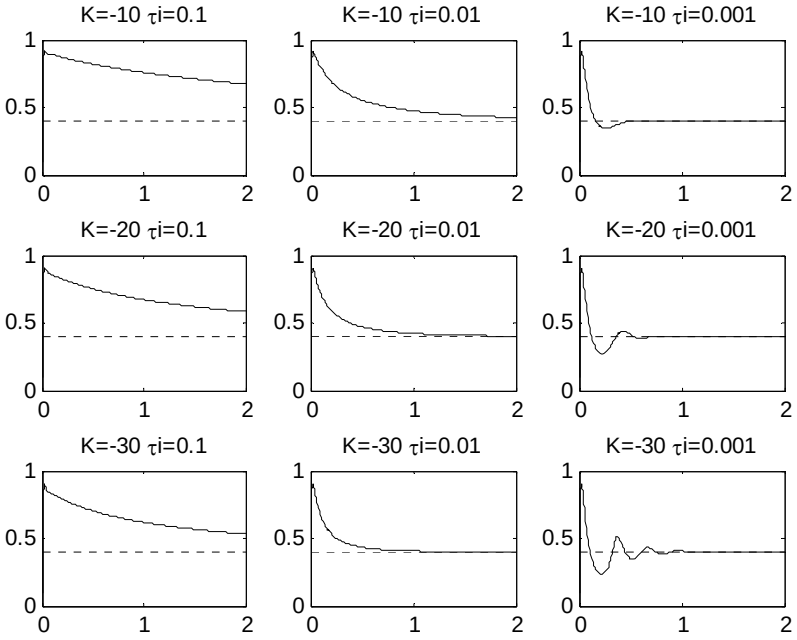

Figure 3.10 Tuning map for PI control of Generation I with $-30 \leq K \leq -10$ [Ns^2] and $0.001 \leq \tau_i \leq 0.1$ [s]. The x-axis shows time [s] and the y-axis differential velocity [ms^{-1}].

The tuning map indicates that an acceptable settling time is obtained with $-30 < K < -20$ [Ns^2] and $0.001 < \tau_i < 0.01$ [s]. A further tuning map with values in these regions is presented in Figure 3.11.

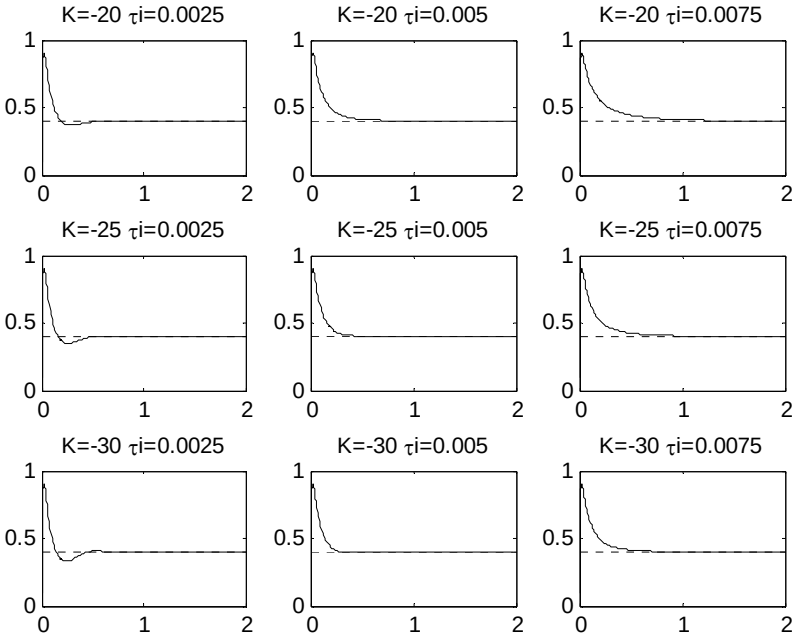

Figure 3.11 Tuning map for PI control of Generation I with $-30 \leq K \leq -20$ [Ns^2] and $0.0025 \leq \tau_i \leq 0.0075$ [s]. The x-axis shows time [s] and the y-axis differential velocity [ms^{-1}].

From the tuning map it can be determined that a proper value for the proportional term is about -25 Ns^2 and that the integral time should be between 0.0025 s and 0.005 s. With this in mind the control error can be studied for different combinations of parameters. Desired performance was found for $K = -26$ Ns^2 and $\tau_i = 0.0036$ s for $v = 20$ ms^{-1}, see Figure 3.12. The system settles after $t_s = 0.19$ s.

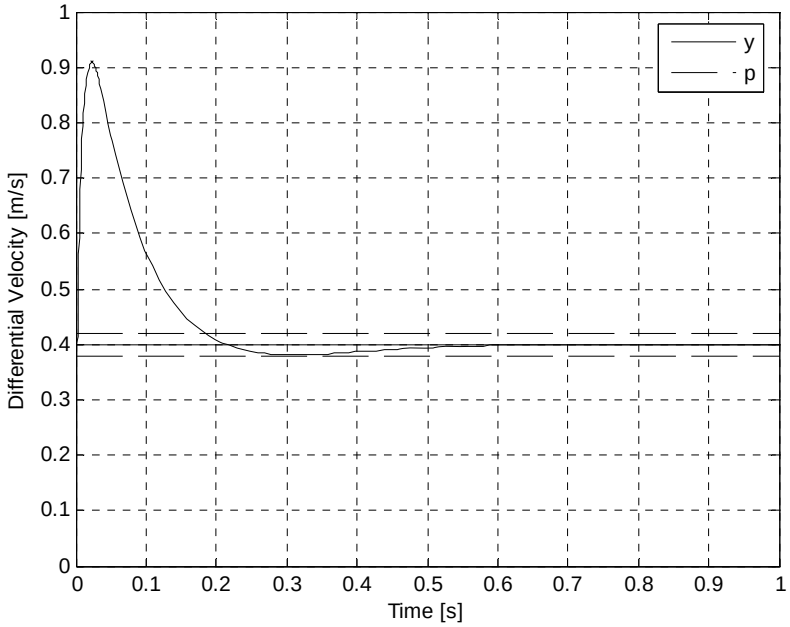

Figure 3.12 Settling behaviour for PI control of Generation I for $v = 20$ ms^{-1} with $K = -26$ Ns^2 and $\tau_i = 0.0036$ s.

As predicted in Section 3.4.1 the behaviour for a smaller initial velocity is harder to control. When the same procedure was preformed for $v_0 = 5$ ms^{-1} it resulted in a smaller integral time to get a desired performance, see Figure 3.13. By this, it can thus be concluded that it would be advantageous to use a gain scheduling for the integral time with respect to the velocity, see Section 3.4.4 for more information.

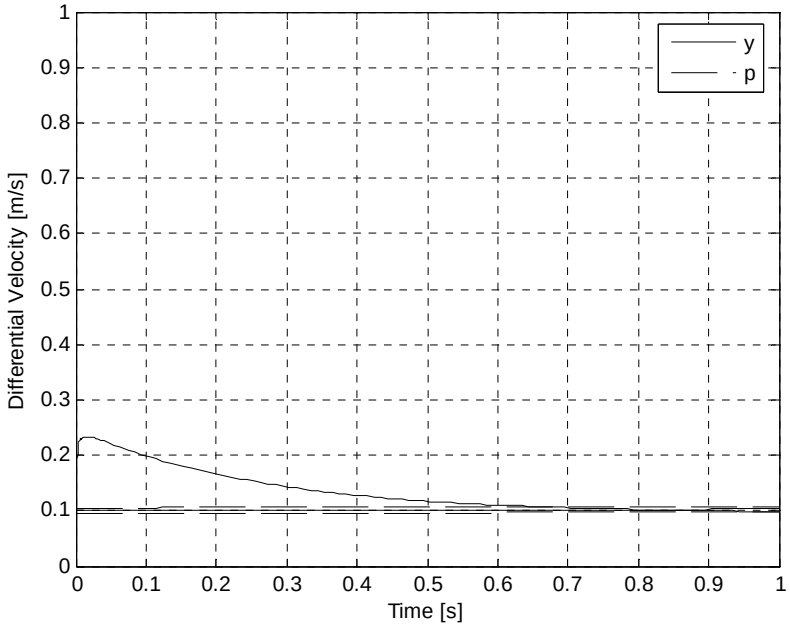

Figure 3.13 Settling behaviour for PI control of Generation I for $v = 5$ ms^{-1} with $K = -26$ Ns^2 and $\tau_i = 0.00066$ s.

A notable difference between high and low initial velocity is that the overshoot will be smaller for a low velocity but the settling time will be longer.

Introducing a derivative action to the controller might improve the closed loop stability. For fixed values on the proportional gain and the integral time respectively a D-part was introduced. For short derivation time the D-part did not add to the stability and for a longer value the system became highly unstable. This behaviour could be predicted because usually a derivative action does not help much when there is a dominant time delay [15].

The controller parameters chosen for Generation I are shown in Table 3.2.

Table 3.2 Controller parameters for Generation I.

	$v = 20$ ms^{-1}	$v = 5$ ms^{-1}
K	-26 Ns^2	-26 Ns^2
τ_i	0.00360 s	0.00066 s

Generation IV

The same method was used for tuning Generation IV. An example of a tuning map that shows the effect of parameter changes on the system can be seen in Figure 3.14.

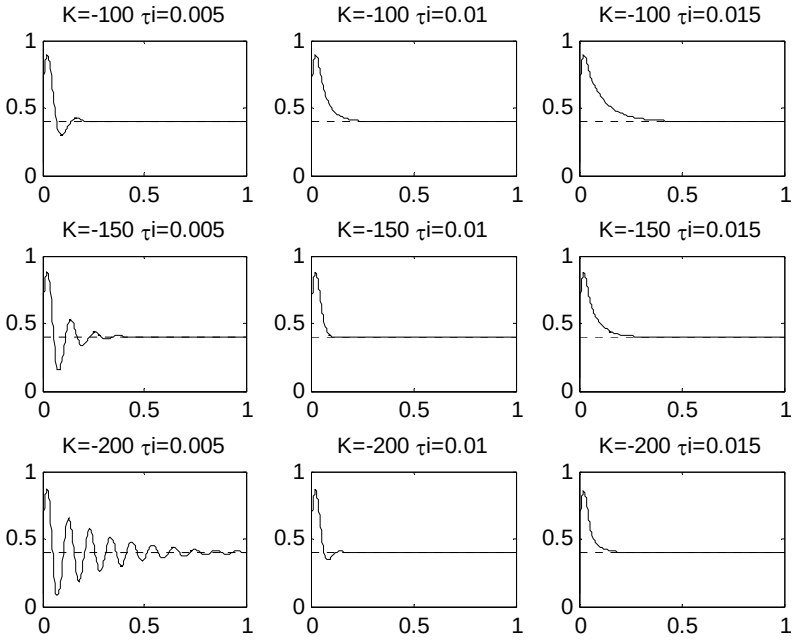

Figure 3.14 Tuning map for PI control of Generation IV with $-10 \leq K \leq -30$ [Ns] and $0.001 \leq \tau_i \leq 0.1$ [s]. The x-axis shows time [s] and the y-axis differential velocity [ms^{-1}].

The parameters were chosen to $K = -150$ Ns and $\tau_i = 0.0093$ s because this gives the shortest settling time t_s. The result can be seen in Figure 3.15.

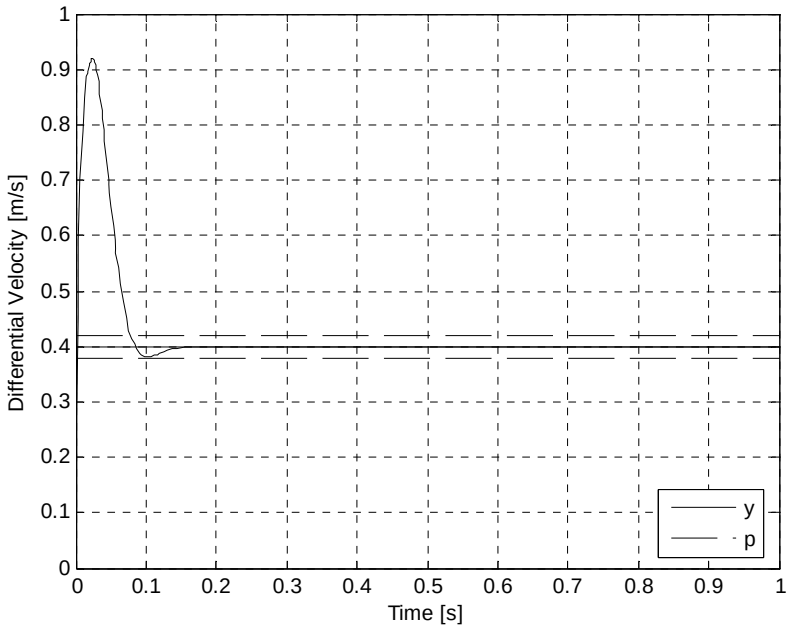

Figure 3.15 Settling behaviour for PI control of Generation IV for $v = 20$ ms^{-1} with $K = $ -150 Ns and $\tau_i = 0.0093$ s.

As in Generation I the behaviour depends highly on the initial velocity of the vehicle and a gain scheduling was therefore used. The settling time could be kept small by choosing a smaller integral time, se Figure 3.16. A better result for small t can be achieved for a larger proportional gain but this gives an instable behaviour if the simulation is performed under a long time.

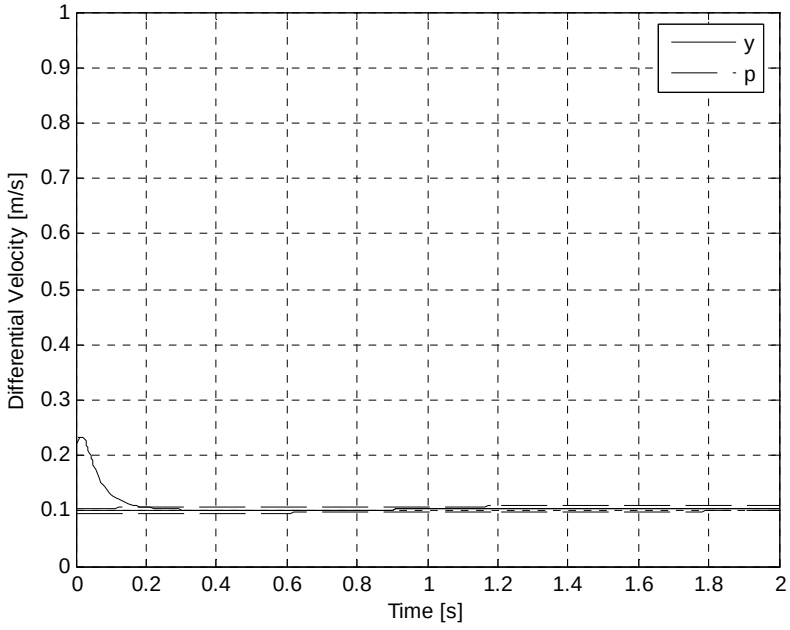

Figure 3.16 Settling behaviour for PI control of Generation IV for $v = 5$ ms^{-1} with $K = $ -150 Ns and $\tau_i = 0.004$ s.

An introduction of a derivative action was also tested for Generation IV but this did not add to the system stability, see reasoning for Generation I above, and was therefore not used.

The chosen values for the controller parameters in Generation IV can be seen in Table 3.3.

Table 3.3 Controller parameters for Generation IV.

	$v = 20$ ms^{-1}	$v = 5$ ms^{-1}
K	-150 Ns	-150 Ns
τ_i	0.0093 s	0.0040 s

3.5 Simulation and Analysis

All the simulations where done in Matlab/Simulink. To solve the initial value problems for the ordinary differential equations the solver *ode23s*, which is based on a modified Rosenbrock formula of order 2, was used. This solver was chosen because it works efficiently at crude tolerances. The step size was set to variable with maximum step size $1e^{-2}$ and an automatic minimum step size. The simulations were performed at tighter tolerances until two consecutive gave the same result. The cruder one was then chosen. The relative tolerance used in the simulations was $1e^{-4}$ and the absolute tolerance was $1e^{-5}$.

3.6 Implementation

As described in Section 1 the purpose of this master thesis is to compare the slip controllers in Generation I and Generation IV by simulations and no real implementation has therefore been done.

4 Results and Discussion

The results from the simulations are presented and discussed in this chapter. Generation I and Generation IV are treated separately but evaluated from the same requirements to enable a well-founded comparison. The requirements on the control system are outlined in the first section of the chapter.

4.1 Requirements

The process signal, y, defined as the difference between the velocity of the front and rear wheels measured in ms^{-1}, should follow the set point signal which is a small percentage of the vehicle longitudinal velocity. If a disturbance acts on the system the controller has to minimize the error between the process signal and the set point signal as fast as possible and prevent a lasting error. The performance of the slip controller was evaluated from three quantities; the integrated absolute error *IAE*, the settling time t_s and the maximum error e_{max}, see Section 3.2 for more information.

A normal driving condition was defined as the case when the vehicle has a constant driveline torque of 1135 Nm. The initial velocity was set to 20 ms^{-1} and 5 ms^{-1} respectively. The vehicle drives up a hill with 14° incline which corresponds to about 25 % inclination. The friction coefficient between the tyres and the surface were 0.8. The time delay from the CAN-bus was set to 20 ms.

4.1.1 Set Point Change

As in Section 3.4.5 the time it takes for the system to settle the response from a set point change due to an initial error in the differential angular velocity is studied. If the velocity is $v = 20 ms^{-1}$ the differential velocity is 0.1 ms^{-1} and the set point signal is 0.4 ms^{-1} at $t = 0$ for the normal driving condition.

4.1.2 Change in Driveline Torque

One possible disturbance to the system is a change in driveline torque. This occurs when the driver steps on the gas. In the simulations the driveline torque was increased from 600 Nm to 1200 Nm after $t = 1$ s.

4.1.3 Change in Friction

Another possible disturbance to the system is a change in friction. On example of this is if the vehicle encounters an ice spot which decreases the friction between the wheels and the surface. The vehicle has the same initial values as in the normal driving conditions. After $t_1 = 1$ seconds the first wheel pair hits an ice spot. Since the vehicle is assumed to move with a constant velocity, the rear wheel pair will reach the ice spot after

$$t_2 = t_1 + \frac{l_a + l_b}{v} \tag{4.1}$$

seconds. Where l_a is the distance from the centre of gravity to the front wheel pair and l_b the distance from the centre of gravity to the rear wheel pair.

In the simulations the friction was dropped from $\mu = 0.8$ to $\mu = 0.4$. The settling time was defined as the time it takes for the system to settle the disturbances for both wheels.

4.1.4 Change in Wheel Radius

The input signal to the controller is the process signal y which is a measured quantity. In reality the angular velocity is measured and then multiplied with a predefined nominal wheel radius that is the same for all wheels. A difference between the real and the nominal radius can occur, e.g., when one tyre is deflated. Simulations were performed with the front wheel effective rolling radius at 95 % of the nominal wheel radius.

4.1.5 Sensitivity to Time Delay from the CAN-bus

The measured signal y is received from the CAN-bus which gives it a time delay. This means that the signal used to calculate the control signal is a delayed value.

4.2 Slip Controller Generation I

The slip controller with the parameter settings in Table 3.2 has been simulated in the above listed driving conditions and evaluated according to the error quantifications introduced in Section 4.1.

4.2.1 Set Point Change

Simulations were done for a vehicle with a Generation I coupling in normal driving conditions, see Section 4.1for a description of the normal driving condition. Since there is an error when the simulations starts it will take some time for the system to settle. A quantification of the error can be seen in Table 4.1.

Table 4.1 Error quantification for normal driving conditions at low and high velocities in Generation I.

	quantification $v = 20$ ms^{-1}	quantification $v = 5$ ms^{-1}
IAE	0.05 ms^{-1}	0.05 ms^{-1}
t_s	0.19 s	0.66 s
e_{max}	0.52 ms^{-1}	0.13 ms^{-1}

The integrated absolute error is sufficiently small although the maximum error, caused by the overshoot, is fairly large. The system settles after 0.19 s which can be considered a reasonable short time. The simulation was also performed at a lower velocity which resulted in a smaller overshoot but a longer settling time.

4.2.2 Change in Driveline Torque

When the driver steps on the gas the wheel spin will be increased which leads to a larger error than before. The system's reaction to an increased driveline torque after 1 s can be seen in Figure 4.1.

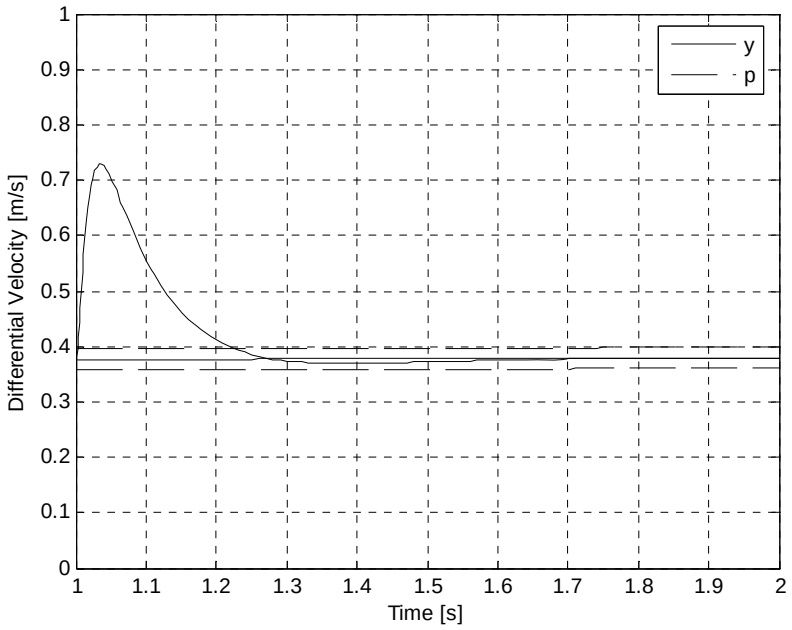

Figure 4.1 Settling behaviour for a change in driveline torque in Generation I.

It can be seen that the system reacts fast to a change in driveline torque and the overshoot is small. A larger step in the driveline torque gives a larger overshoot but the settling time will still be sufficiently short. The quantifications of the error are presented in Table 4.2.

Table 4.2 Error quantification for a change in driveline torque in Generation I.

	quantification
IAE	0.01 ms^{-1}
t_s	0.23 s
e_{max}	0.35 ms^{-1}

4.2.3 Change in Friction

If the vehicle encounters an ice spot the front wheel will start to spin first and then, when the rear wheel reaches the ice spot it will also start to spin. This means that the error first will increase when the first wheel spins and then decrease when the second wheel spins. The maximum error is relatively small and the integrated absolute error is still kept small. The values of the error quantifications are shown in Table 4.3.

Table 4.3 Error quantification for a change in friction in Generation I.

	quantification
IAE	0.05 ms^{-1}
t_s	0.25 s
e_{max}	0.50 ms^{-1}

When the front tyre starts to spin the controller will distribute more of the driveline torque to the rear tyre that has better adhesion to the surface and so maximize the total longitudinal force. The amount of the driveline torque that is transferred to the rear shaft when the vehicle hits a slippery spot is showed in Figure 4.2. Here the settling behaviour can also be seen.

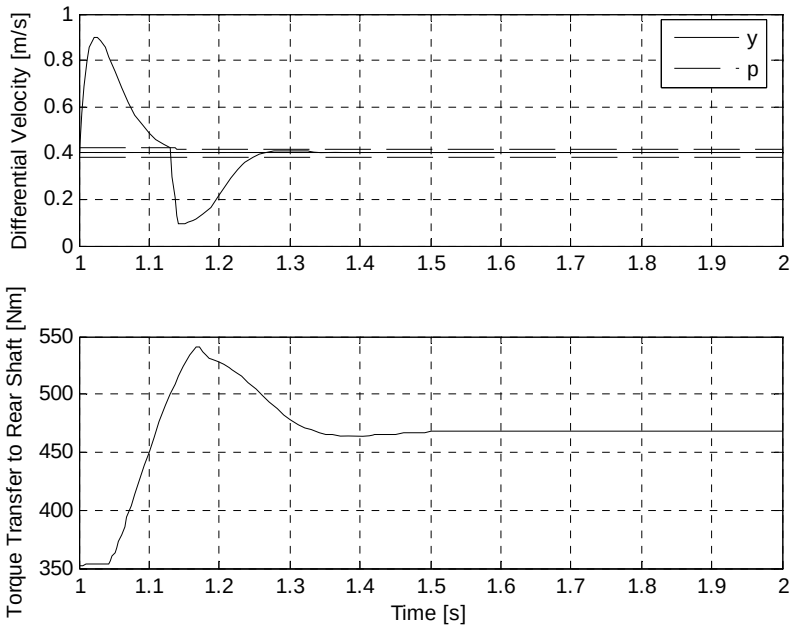

Figure 4.2 Settling behaviour for a change in friction and the amount of driveline torque transferred to the rear shaft in Generation I.

4.2.4 Change in Wheel Radius

The initial condition problem was investigated again but with a change in the front wheel radius. The result of the simulation can be seen in Figure 4.3 and compared to the settling behaviour in the normal driving condition in Figure 3.12. Note however, that the overshoot for the deflated tyre reaches a more than twice as high value.

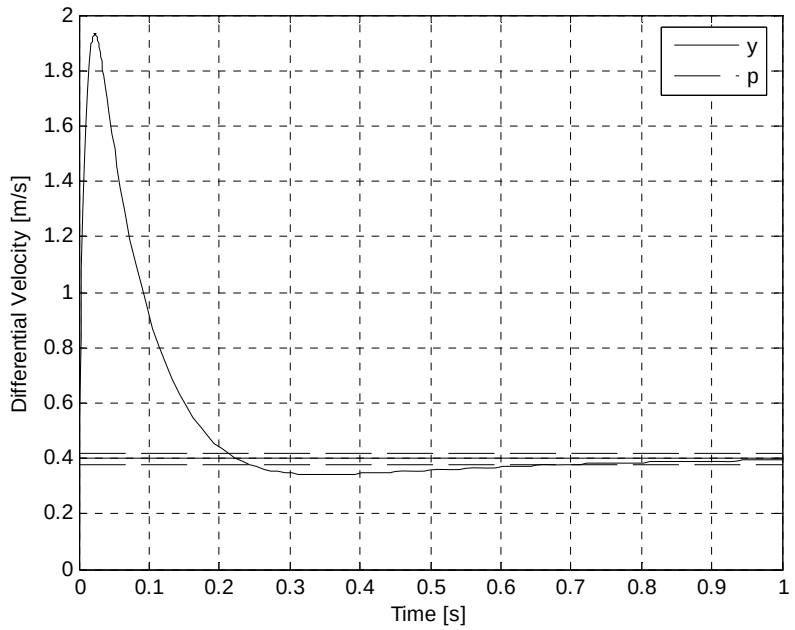

Figure 4.3 Settling behaviour for deflated tyre in Generation I.

A deflated tyre will, as can be seen in Table 4.4, lead to a large initial error.

Table 4.4 Error quantification for a deflated tyre in Generation I.

	quantification
IAE	0.16 ms^{-1}
t_s	0.72 s
e_{max}	1.54 ms^{-1}

4.2.5 Sensitivity to Time Delay from the CAN-bus

To get an idea of how the time delay from the CAN-bus affects the system, the simulations were done with the same control parameters as before, but with a larger time delay. This results in oscillations before the system settles as can be seen in Figure 4.4.

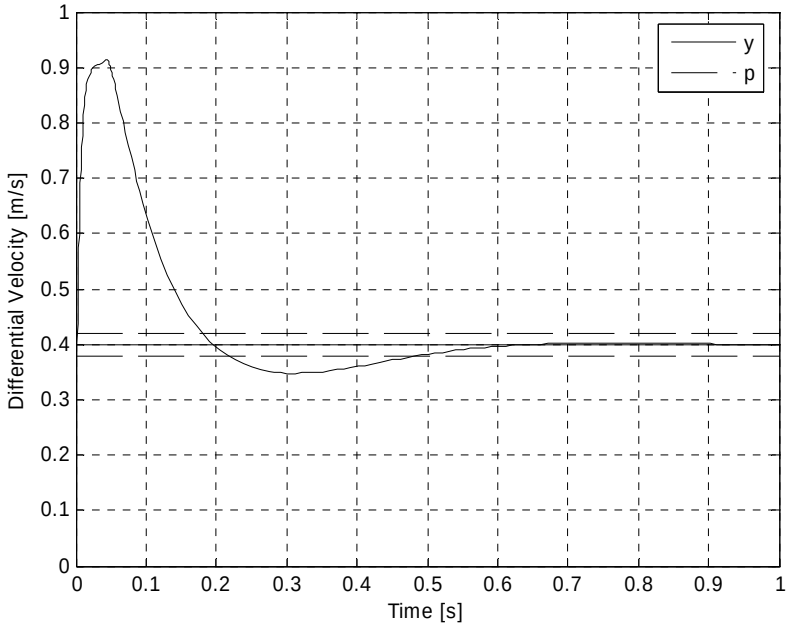

Figure 4.4 Settling behaviour for time delay from the CAN-bus of 40 ms in Generation I for $v = 20$ ms^{-1}.

For a vehicle driving with a high velocity at $v = 20$ ms^{-1} the settling will be longer for a longer time delay from the CAN-bus but the maximum error and the integrated absolute error will be approximately the same as before. When the vehicle is driving with a lower velocity at $v = 5$ ms^{-1} the maximum error will be as before. The settling time and the integrated absolute error however have increased significantly. The quantifications of the error are displayed in Table 4.5 and can be compared to the values in Table 4.1.

Table 4.5 Error quantification for a time delay from the CAN-bus of 40 ms in Generation I.

	quantification $v = 20$ ms^{-1}	quantification $v = 5$ ms^{-1}
IAE	0.06 ms^{-1}	0.22 ms^{-1}
t_s	0.49 s	3.92 s
e_{max}	0.53 ms^{-1}	0.13 ms^{-1}

4.3 Slip Controller Generation IV

The slip controller in Generation IV has been simulated with the control parameters in Table 3.3 in the same driving conditions as Generation I to make a comparison possible.

4.3.1 Set Point Change

The vehicle was simulated in so called normal driving conditions with a set point change in $t = 0$, refer to Section 4.1 and the error quantifications were notated and stored into Table 4.6.

Table 4.6 Error quantification for normal driving conditions at low and high velocity in Generation IV.

	quantification $v = 20$ ms^{-1}	quantification $v = 5$ ms^{-1}
IAE	0.02 ms^{-1}	0.02 ms^{-1}
t_s	0.08 s	0.12 s
e_{max}	0.52 ms^{-1}	0.13 ms^{-1}

As in Generation I it can be seen that when the vehicle starts at a lower velocity the settling time will be longer but the maximum error will be smaller. This agrees with the reasoning in Section 3.4.1. The difference between the two compared systems is that Generation IV settles faster than Generation I. This can be explained by the differences in the coupling. In Generation I there has to be a sufficiently large oil flow, and therefore also differential angular velocity, to be able to receive a certain torque transfer. The time it takes for this flow to be generated makes the system slower. Refer to Section 2.2.1 for further explanation.

4.3.2 Change in Driveline Torque

A step in the driveline torque only generates a small overshoot in Generation IV, which can be seen in Figure 4.5.

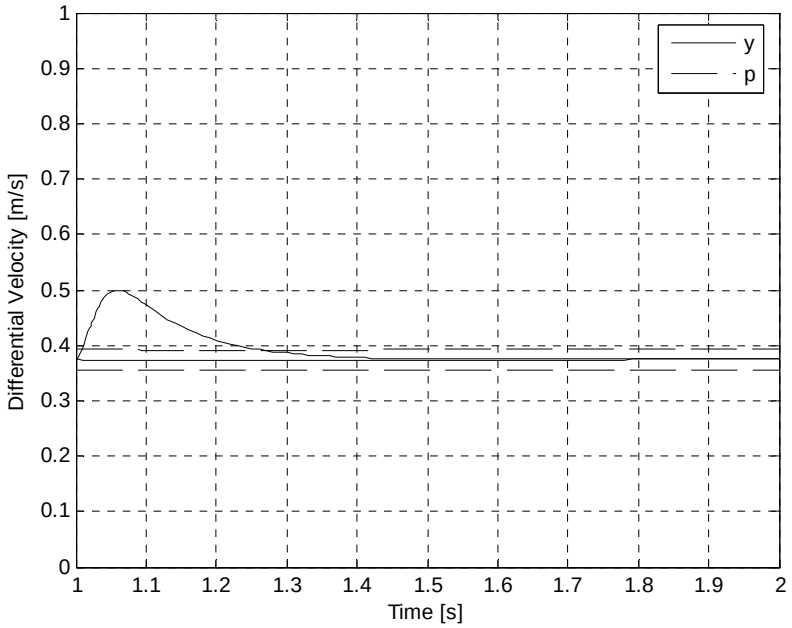

Figure 4.5 Settling behaviour for a change in driveline torque in Generation IV.

The settling time is approximately equal for the same step in driveline torque in Generation I and IV but the latter has a smaller overshoot. The quantifications of the error are displayed in **Table 4.7**. The fact that Generation I is not slower in this case might depend on that an oil flow has already been generated to counteract the error at the time $t = 0$. For Generation IV however, there is always a time delay in the coupling.

Table 4.7 Error quantification for a change in driveline torque in Generation IV.

	quantification
IAE	0.03 ms^{-1}
t_s	0.27 s
e_{max}	0.13 ms^{-1}

4.3.3 Change in Friction

A change in friction in Generation IV gives a oscillating system which does not settle during simulations for 10 minutes. The definable error quantifications can be found in Table 4.8.

Table 4.8 Error quantification for a change in friction in Generation IV.

	quantification
IAE	-
t_s	-
e_{max}	0.7 ms^{-1}

Looking at the graph in Figure 4.6 it can be determined that the slippery spot generates a unstable behaviour for Generation IV, note that the y-axis in Figure 4.6 is scaled differently than in Figure 4.2.

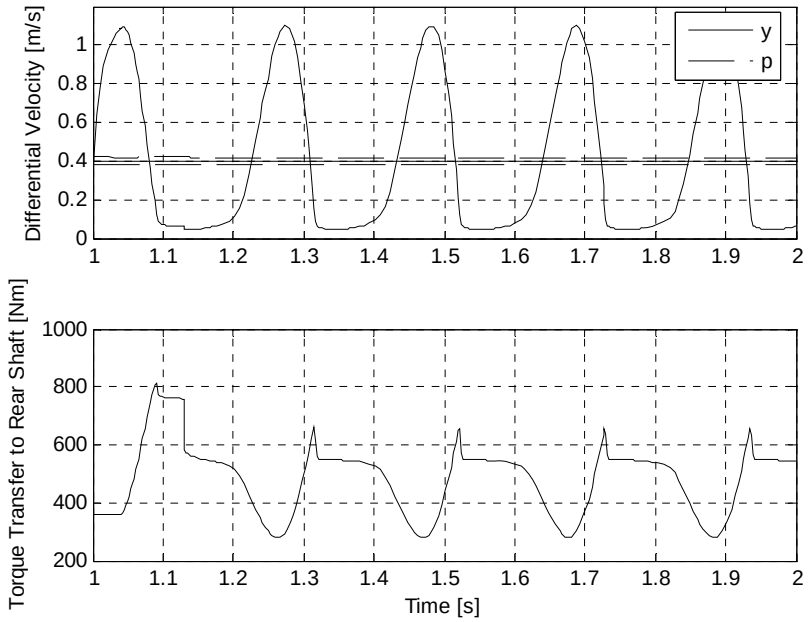

Figure 4.6 Settling behaviour for a change in friction and the amount of driveline torque transferred to the rear shaft in Generation IV.

The system may be made stable by increasing the integral time but this makes the system slow and the oscillations will not disappear completely. The oscillations are caused by the time delay. When the system was simulated without the delay the oscillations could easily be avoided.

4.3.4 Change in Wheel Radius

As before the system was simulated for a change in the actual wheel radius on the front wheel. This results in larger oscillations before the system settles as can be seen in Figure 4.7. It takes the system 0.1 s longer to settle with the smaller wheel radius.

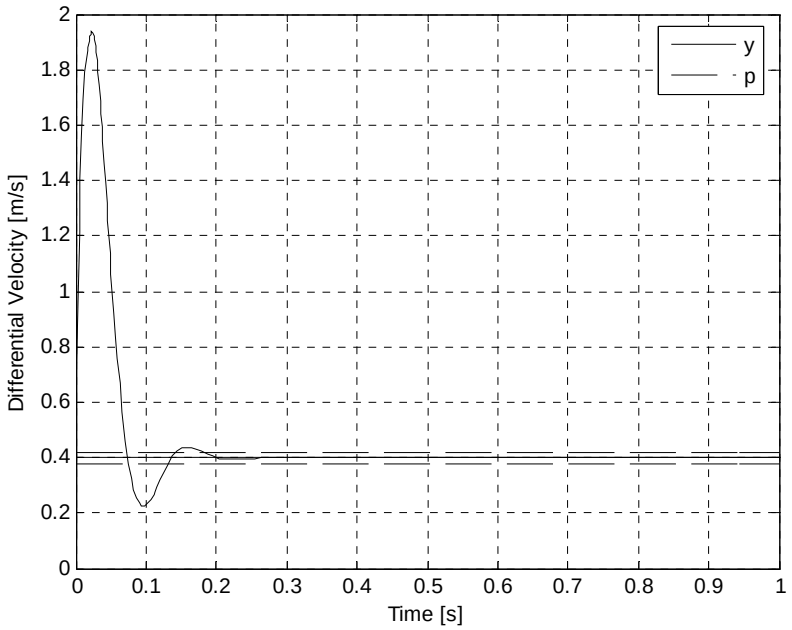

Figure 4.7 Settling behaviour for deflated tyre in Generation IV.

The overshoot is approximately the same as for Generation I but the system settles faster for Generation IV, this can be explained in the same way as for normal driving conditions, se Section 4.1.The quantifications of the errors are displayed in Table 4.9.

Table 4.9 Error quantification for a deflated tyre in Generation IV.

	quantification
IAE	0.08 ms^{-1}
t_s	0.18 s
e_{max}	1.54 ms^{-1}

The simulations show that the two compared systems have approximately the same behaviour to changes in the actual wheel radius irrespective of the amount of change and if the front or the rear wheel is changed.

4.3.5 Sensitivity to Time Delay from the CAN-bus

If the delay from the CAN-bus is increased to 40 ms the system will become less damped as can be seen in Figure 4.8.

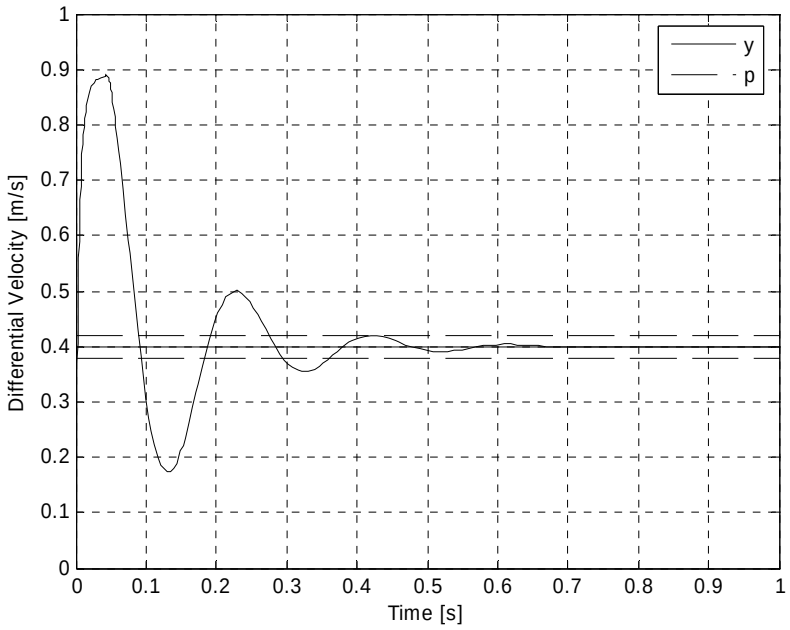

Figure 4.8 Settling behaviour for time delay from the CAN-bus of 40 ms in Generation IV for $v = 20$ ms^{-1}.

For the same control parameters as in Table 3.2 the system will have the error quantifications as in Table 4.10. These values are similar to the ones determined for Generation I. The difference is that if the system is simulated for a longer time period Generation IV will become unstable.

Table 4.10 Error quantification for a time delay from the CAN-bus of 40 ms in Generation IV for v = 20 ms^{-1}.

	quantification
IAE	0.06 ms^{-1}
t_s	0.43 s
e_{max}	0.53 ms^{-1}

It is possible to retune the controller parameters to fit a longer delay from the CAN-bus. The controller parameters where then chosen as in Table 4.11. The result is presented in Table 4.12 and gives a stable system for 600 s which was considered a sufficiently long time period. This gives a settling behaviour similar to the one with a time delay of 20 ms, refer to Table 4.6.

Table 4.11 Controller parameters for a delay from the CAN-bus of 40 ms in Generation IV for v = 20 ms^{-1}.

	$v = 20$ ms^{-1}
K	-150 Ns
τ_i	0.016 s

Table 4.12 Error quantification for a time delay from the CAN-bus of 40 ms in Generation IV for v = 20 ms^{-1}.

	quantification
IAE	0.04 ms^{-1}
t_s	0.09 s
e_{max}	0.53 ms^{-1}

Generation IV is hence more sensitive to a longer time delay. The likely explanation for this is that there is a mechanical system feedback in Generation I. When the differential angular velocity is reduced due to the transferred torque, the oil flow produced by the hydraulic piston pump will decrease and thus decreasing the transferred torque, refer to Equation (3.5). However, simulations show that with the new parameter settings chosen, see Table 4.11, Generation IV will be stable for at least 600 s and have approximately the same behaviour as with a shorter time delay.

To secure this further the test where the driver steps on the gas was simulated again but with a longer time delay from the CAN-bus and the new controller parameters. The result can be seen in Figure 4.9. The overshoot will be larger than for the shorter time delay but the settling time is still reasonable and the system stays stable for at least 600 s. The controller can be said to handle a change in driveline torque also for long time delay from the CAN-bus.

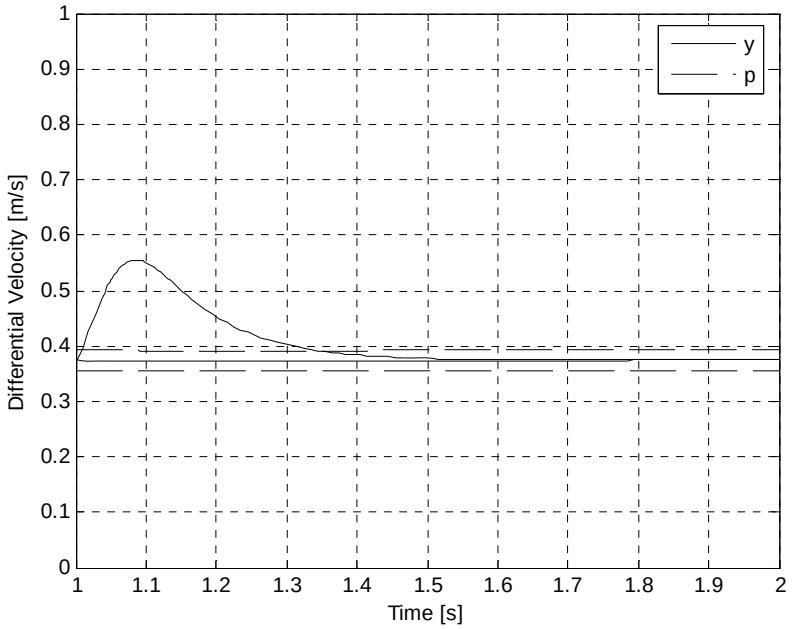

Figure 4.9 Settling behaviour for change in driveline torque and time delay from the CAN-bus of 40 ms in Generation IV for $v = 20$ ms^{-1}.

When the vehicle drives with a lower velocity the system will also become unstable for a time delay from the CAN-bus of 40 ms with the parameter settings in Table 3.3. Retuning them to handle these new circumstances gave the result presented in Table 4.13. This gives a stable system for at least 600 s and error quantifications, see Table 4.14, that are approximately the same as for a shorter time delay, compare to Table 4.6.

Table 4.13 Controller parameters for a delay from the CAN-bus of 40 ms in Generation IV for v = 5 ms^{-1}.

	$v = 5$ ms^{-1}
K	-150 Ns
τ_i	0.006 s

Table 4.14 Error quantification for a time delay from the CAN-bus of 40 ms in Generation IV for $v = 5$ ms^{-1}.

	quantification
IAE	0.03 ms^{-1}
t_s	0.20 s
e_{max}	0.13 ms^{-1}

It is hence possible to retune the controller in Generation IV to handle a time delay from the CAN-bus of 40 ms reasonable well for a change in set point and driveline torque. However, the controller will still not handle a change in friction but will become unstable.

5 Conclusions

With the discussion in the former chapter as a basis the slip controllers for the HLSC Generation I and IV are compared and the conclusions are presented below.

When settling the response of a set point change caused by an initial error the slip controller in Generation I and IV approximately have the same overshoot. The difference is that it takes Generation I a longer time to settle. The difference in settling time is larger for a lower vehicle velocity. The explanation for why the slip controller in Generation I settles slower lies in the coupling dynamics. For the system to be able to transfer the desired torque there has to be a sufficiently large oil flow which is approximately proportional to the differential angular velocity. The time it takes for this flow to be generated makes the system slower.

To enable a further comparison between the slip controllers disturbances were introduced in the simulations. When the driveline torque was increased the settling time was more or less the same for Generation I and IV but the prior has a larger overshoot. As a further disturbance the friction between the tyres and the surface was decreased to simulate a ice spot on the road. Generation I recovers from the disturbance fast enough but Generation IV becomes unstable.

For a change of the front wheel radius, e.g., caused by a deflated tyre, the settling time for the initial value problem will be longer then before for both generations. If the difference becomes too large the controller will settle the system at the wrong differential velocity. The simulations show that Generation I and IV behave similar sensitive to these changes.

When the time delay from the CAN-bus was increased both Generation I and IV took a longer time to settle but Generation IV was more sensitive under longer simulations. This may be explained by the mechanical system feedback in Generation I. To ensure a stable behaviour for Generation IV the control parameters where retuned. These new settings allows the system to have approximately the same performance as for the shorter time delay.

To sum up it can be said that the slip controller in Generation IV can be made faster due to less embedded delay in the coupling. Generation I on the other side is more robust to changes in friction between the tyres and the surface and is more stable for a longer time delay from the CAN-bus. However, in the simulations performed Generation IV was stable for at least ten minutes with a time delay of 40 ms for a change in set point and driveline torque.

Bibliography

[1] Kiencke, Uwe & Nielsen, Lars (2000). *Automotive Control Systems, For Engine, Driveline, and Vehicle.* Springer-Verlag, Berlin, Heidelberg.

[2] Nohau News no. 1/2006 (2006). *Innovativ fordonsteknologi* [www]. Information from <http://www.nohau.se/newsdesk/news/2006/wNohau_news1_2006.pdf> 07/02/06.

[3] Haldex News Issue II (2000). *Swedish racetracks lead to Haldex LSC p.2* [www]. Information from <http://www.haldex-traction.com/download_material/pdf-files/haldex_news_issue2.pdf> 30/01/06

[4] Haldex Traction AB (2006). *Technical Information* [www]. Information from <http://www.haldex-traction.com> 25/01/06.

[5] Jönsson, Bengt & Lundgren, Torkel (1999). *Pressure Control of Haldex Limited Slip Coupling.* Department of Automatic Control, Lund Institute of Technology.

[6] Presentationsmaterial, Produktutbildning (2005). Haldex Traction Systems.

[7] Nilsson, Staffan (2004). *Linear Pressure Controller for HLSC Specification.* Reg. No. 2002510. Haldex Traction Systems.

[8] Jönsson, Bengt (2005). *Generation 4 Slip Controller Report*. Reg. No. 20040388. Haldex Traction Systems.

[9] Miller, Shannon et al. (2001). Calculating Longitudinal Wheel Slip and Tire Parameters Using GPS Velocity. *Proceedings of the American Control Conference Arlington*, Virginia June 2001, p. 1800-1805.

[10] Mitschke, Manfred (1990). *Dynamik der Kraftfahrzeuge, Band C: Fahrverhalten.* 2nd ed. Springer-Verlag, Berlin.

[11] Pacejka, Hans (2002). *Tyre and Vehicle Dynamics.* Butterworth-Heinemann, Oxford.

[12] Svendenius, Jacob & Wittenmark, Björn (2003). *Review of Wheel Modeling and Friction Estimation*. Department of Automatic Control, Lund Institute of Technology.

[13] Jaschke, Klaus Peter (2002). *Lenkregler für Fahrzeuge mit hoher Schwerpunktlage.* Fakultät für Maschinenbau und Elektrotechnik der Technischen Universität Carolo-Wilhelmina zu Braunschweig [www]. Information from <http://www.biblio.tu-bs.de/ediss/data/20020627b/20020627b.pdf> 03/04/06.

[14] Slotine, Jean-Jacques & Li, Weiping (1991). *Applied Nonlinear Control.* Prentice-Hall, Upper Saddle River.

[15] Åström, Karl Johan & Hägglund, Tore (1995). *PID Controllers: Theory, Design and Tuning.* 2nd ed. Instrumental Society of America, Research Triangle Park.

[16] Institutionen för systemteknik (ISY) Linköpings universitet (2001). *Introduktion till SIMULINK, September 2001* [www]. Information from <http://www.control.isy.liu.se/student/tsrt38/matlab/Simulink_intro.pdf> 05/05/06.

[17] Volvo Personvagnar AB (2006). *Volvo S40 AWD, Tekniska data* [www]. Information from <www.volvocars.se/modelsMY07/s40/techSpec.htm> 30/05/06.

[18] Råde, Lennart & Westergren, Bertil (1990). *Beta: Mathematics Handbook.* 2nd ed. Studentlitteratur, Lund.

[19] Åström, Karl Johan & Wittenmark, Björn (1997). *Computer-Controlled Systems.* 3rd ed. Prentice Hall, Upper Saddle River.

[20] Glad, Torkel & Ljung, Lennart (1989). *Reglerteknik, Grundläggande teori.* 2nd ed. Studentlitteratur, Lund.

Appendix A: Notation

Symbols	Description	Unit
A	Frontal area of the vehicle	m^2
a	Set point weighting parameter	-
b	Set point weighting parameter	-
C_w	Coefficient of wind resistance	-
C_x	Effective longitudinal stiffness	N
c	Coupling constant HLSC Generation I	$\frac{\mathrm{Nm}}{\mathrm{rad}}$
F_d	Aerodynamic drag	N
F_x	Longitudinal force	N
F_z	Tyre normal load	N
g	Gravitational acceleration	$\frac{\mathrm{m}}{\mathrm{s}^2}$
J_i	Wheel-tyre assembly inertia	$\mathrm{kg} \cdot \mathrm{m}^2$
K	Controller gain, Generation I	Ns^2
K	Controller gain, Generation IV	Ns
k	Set-point factor	-
l_a	Distance from the centre of gravity to the front wheel pair	m
l_b	Distance from the centre of gravity to the rear wheel pair	m
m	Vehicle body mass	kg
N	Derivative approximation parameter	-

P	Pressure	Pa
R_{ei}	Effective rolling radius	m
T_d	Calculated desired torque	Nm
T_{drive}	Driveline torque	Nm
T_i	Torque applied to the front and rear shaft	Nm
u	Controller output, Generation I	$\frac{\text{Nm}}{\left(\text{rad}\cdot\text{s}^{-1}\right)}$
u	Controller output, Generation IV	Nm
v_i	Wheel speed for front and rear shaft	$\frac{\text{m}}{\text{s}}$
v_x	Vehicle longitudinal velocity	$\frac{\text{m}}{\text{s}}$
Q	Oil flow	$\frac{\text{m}^3}{\text{s}}$
z_i	Quantity applied at front ($\text{i}=1$) or rear ($\text{i}=2$) shaft	
$\dot{z}$	$\frac{\text{dq}}{\text{dt}}$	
$\mathbf{z}$	Vector	
$\mathbf{Z}$	Matrix	

β	Incline angle	rad
Δv	Process signal	$\frac{\text{m}}{\text{s}}$
Δv_{sp}	Set point signal	$\frac{\text{m}}{\text{s}}$
δ	Stiffness of the HLSC	$\frac{\text{Pa}}{\left(\text{m}^3\cdot\text{s}^{-1}\right)}$
λ_i	Slip at front and rear shaft	-

μ	Friction co-efficient	-
ρ	Density of the air	$\frac{kg}{m^3}$
τ	Coupling constant HLSC Generation IV	s
τ_d	Controller derivative time constant	s
τ_i	Controller integral time constant	s
τ_t	Controller tracking time constant	s
ω_i	Angular velocity at front and rear shaft	$\frac{rad}{s}$

Abbreviations

ABS	Anti-lock Braking System
AWD	All Wheel Drive
CAN	Controller Area Network
ESP	Electronic Stability Program
HLSC	Haldex Limited Slip Coupling
IAE	Integrated Absolute Error
IAE	Society of Automotive Engineers
TCS	Traction Control System

Appendix B: Glossary

actuator ställdon

adhesion vidhäftning

circumference omkrets

clutch koppling

deflect avlänka, avböja

disc clutch lamellkoppling

inflation pressure ringtryck

multi-plate clutch lamellkoppling

piston kolv

propeller shaft kardanaxel

rim fälg

set point börvärde, referensvärde

shaft axel

slip spinna

torque vridmoment

traction dragkraft

transmission växellåda

tread däckmönster

throttle valve strypventil

Appendix C: Simulation Models in Matlab/Simulink

C.1 Basic Structure of Generation I

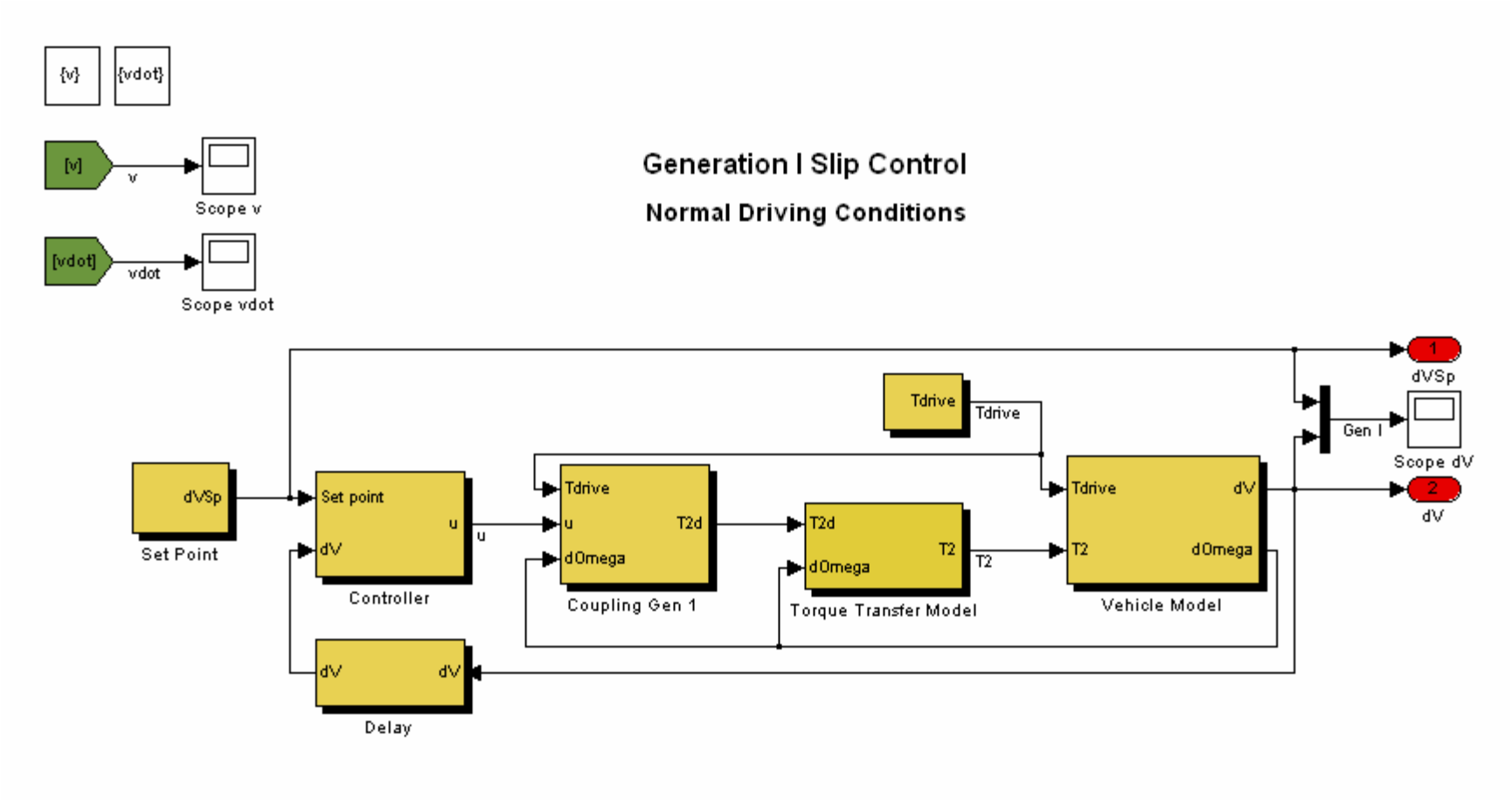

C.2 Basic Structure of Generation IV

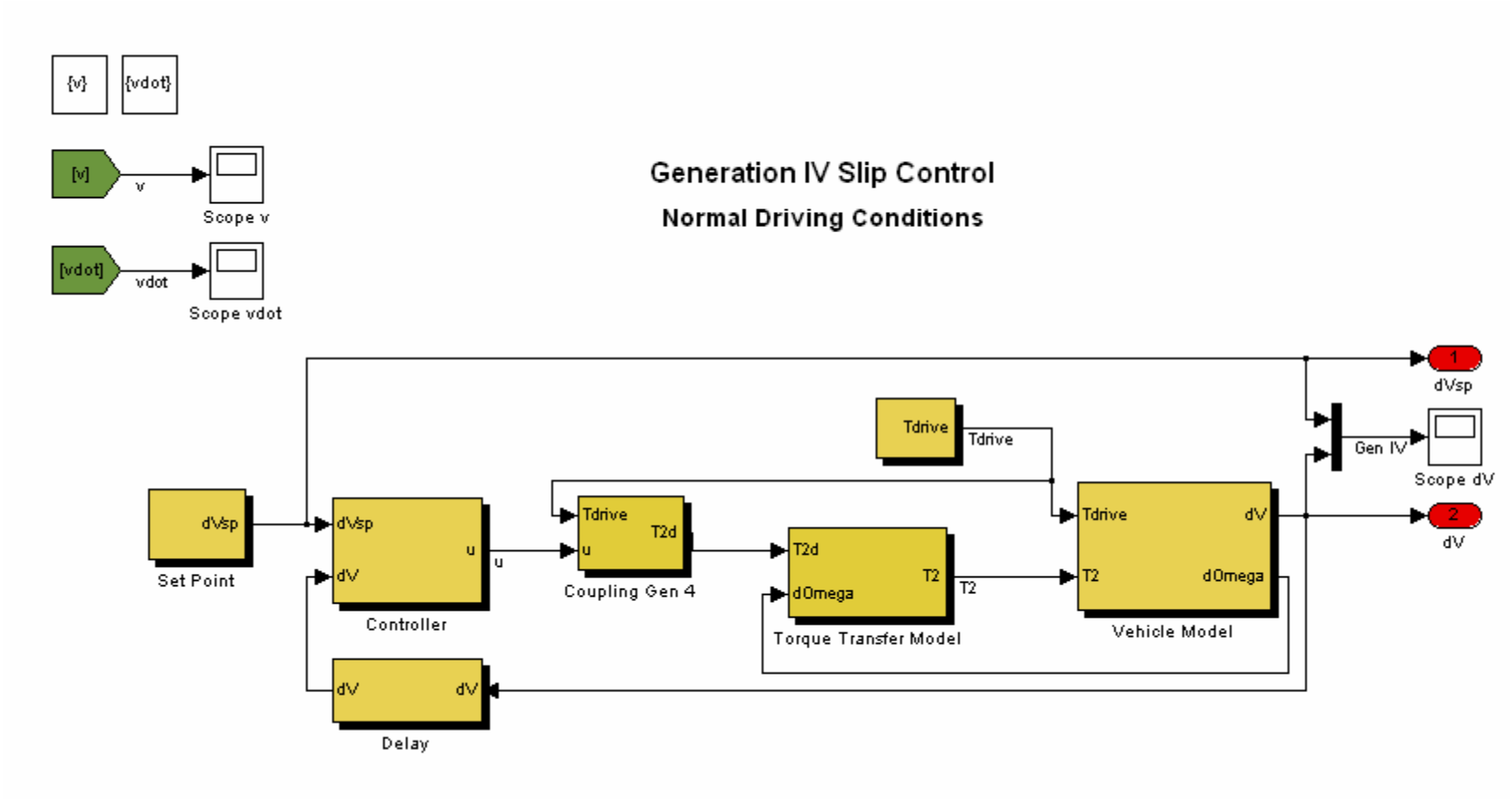

C.3 Vehicle Model

C.3.1 Basic Structure

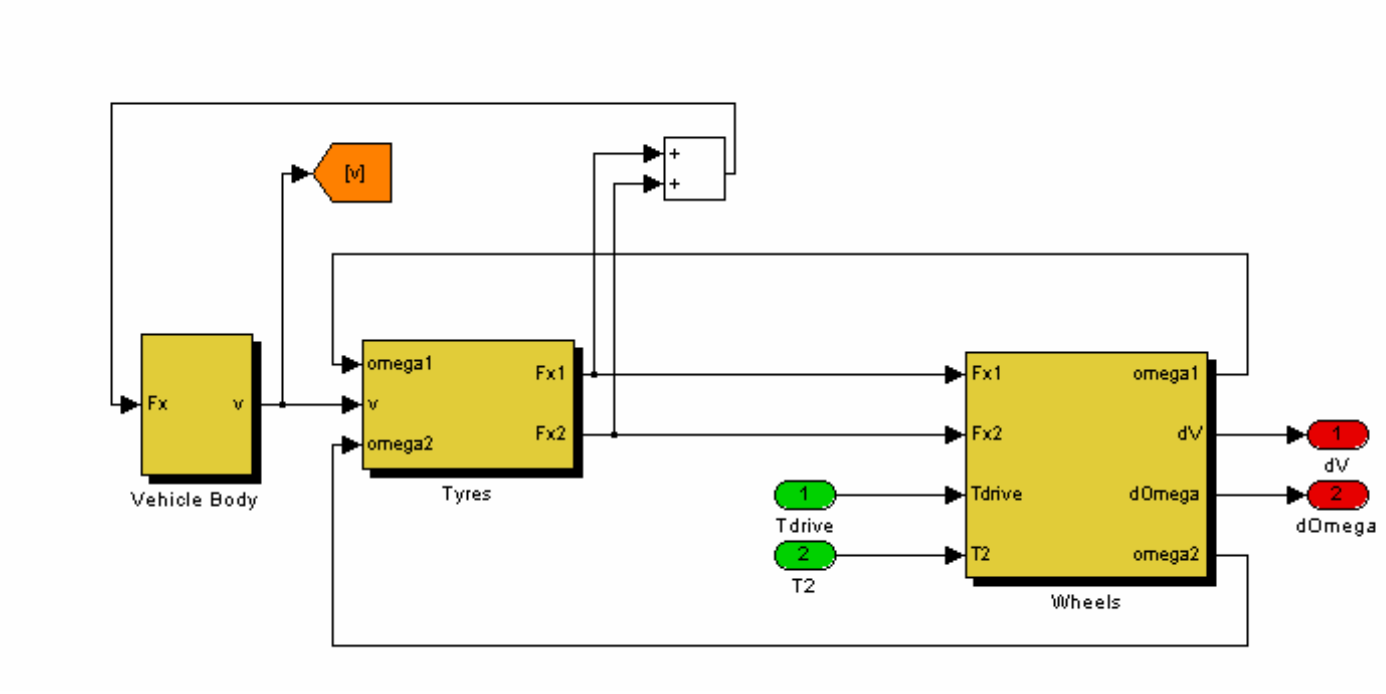

C.3.2 No Division By Zero

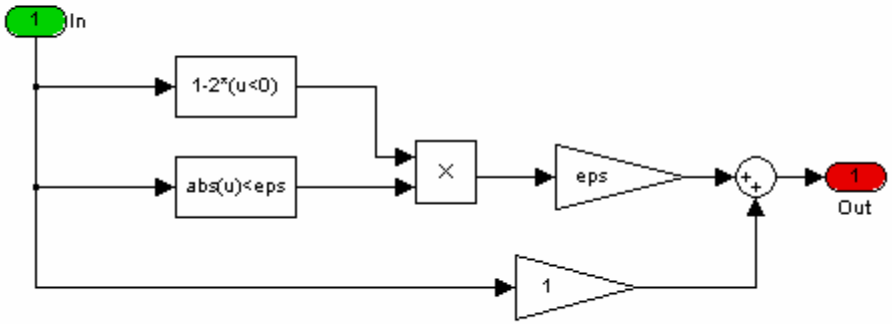

C.3.3 Vehicle Body

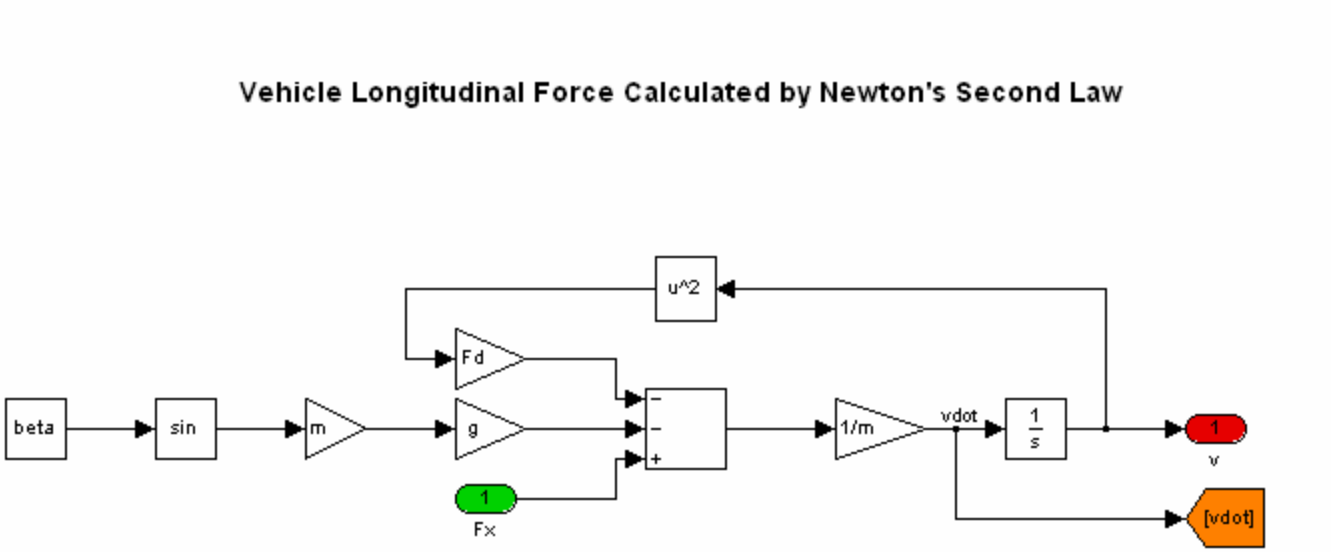

C.3.4 Wheels

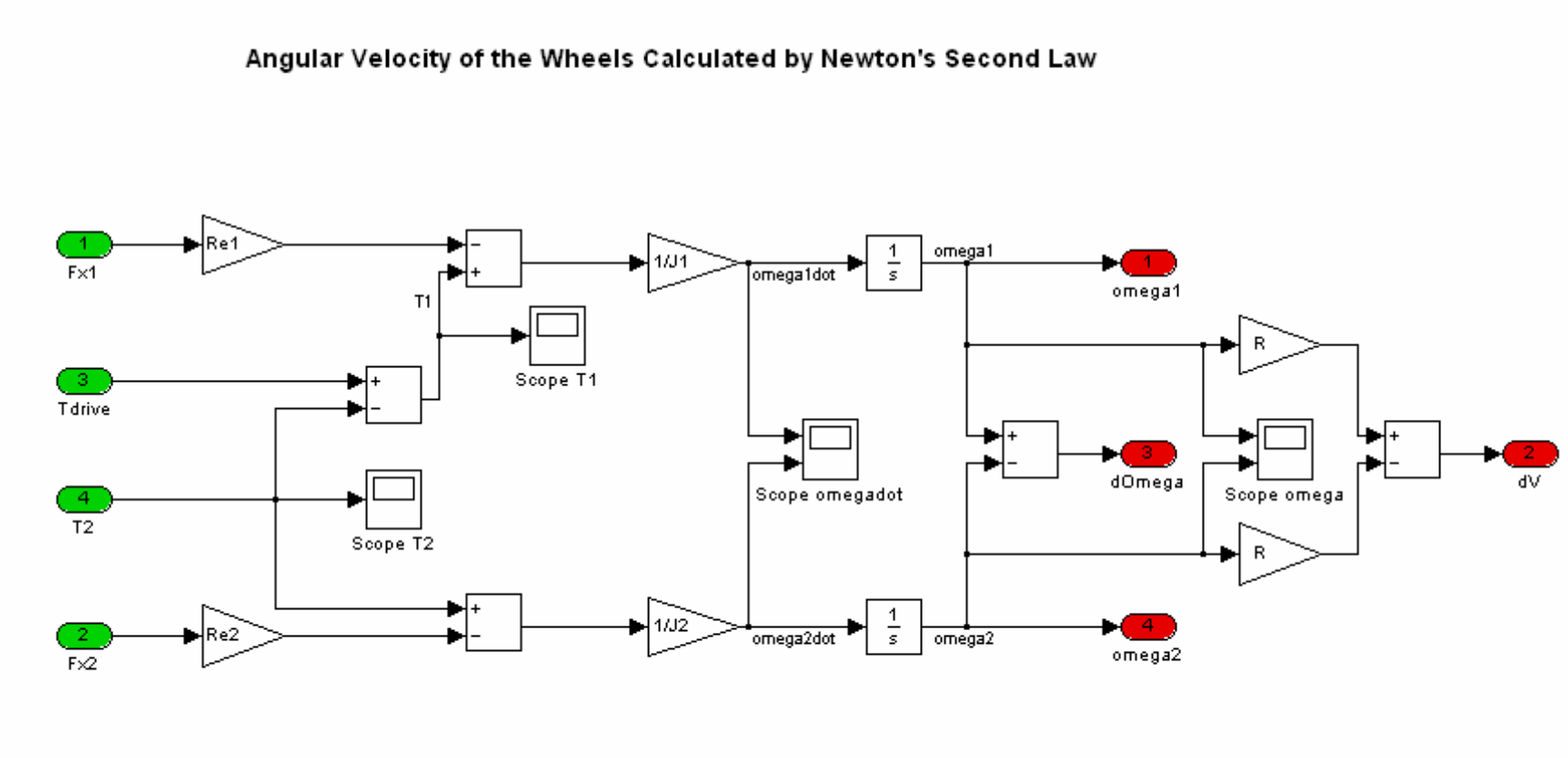
Angular Velocity of the Wheels Calculated by Newton's Second Law
1
Fx1
Re1
T1
Scope T1
3
Tdrive
4
T2
Scope T2
2
Fx2
Re2
1/J1
omega1dot
1/J2
omega2dot
Scope omegadot
1
s
omega1
omega2
1
omega1
3
dOmega
R
R
Scope omega
2
dV
4
omega2

C.3.5 Tyres

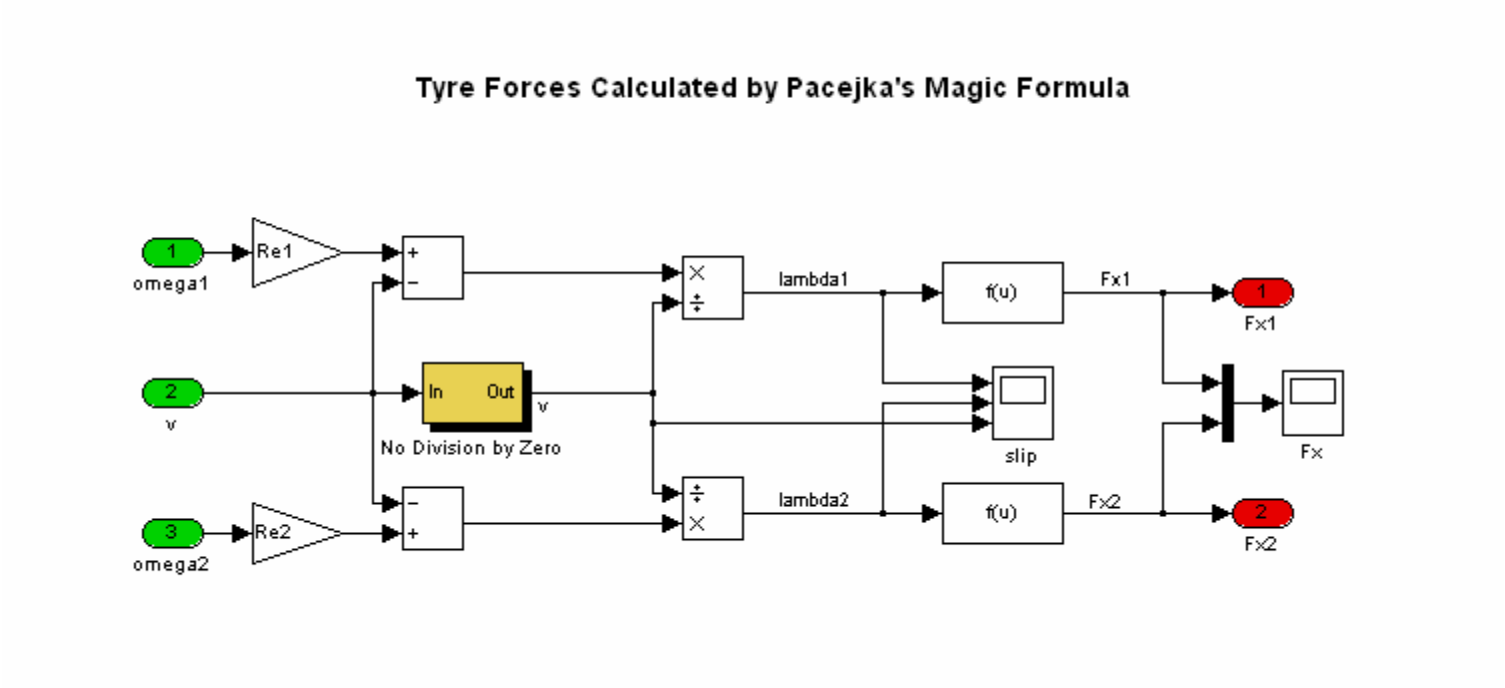
Tyre Forces Calculated by Pacejka's Magic Formula
1
omega1
Re1
2
v
3
omega2
Re2
In
Out
v
No Division by Zero
lambda1
lambda2
f(u)
f(u)
Fx1
Fx2
slip
1
Fx1
2
Fx2
Fx

C.4 Torque Transfer Model

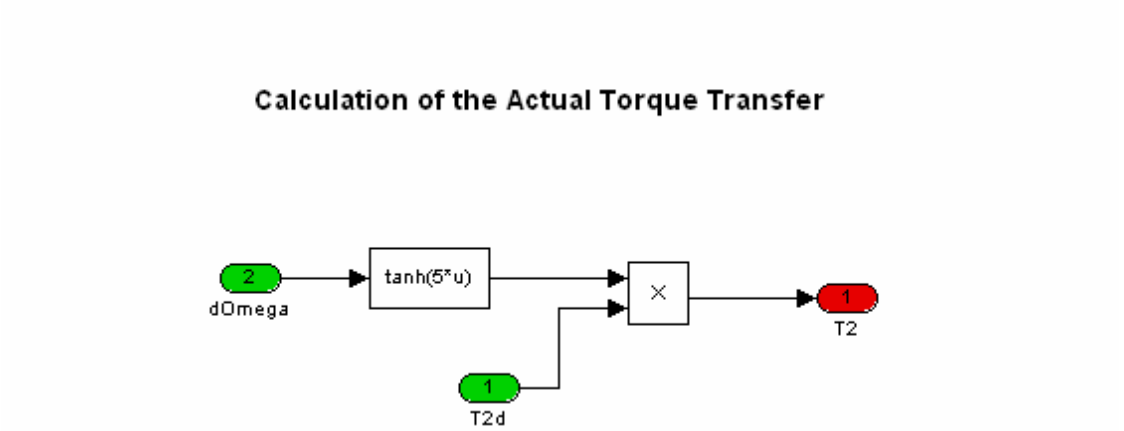

C.5 Haldex Limited Slip Coupling

C.5.1 Generation I

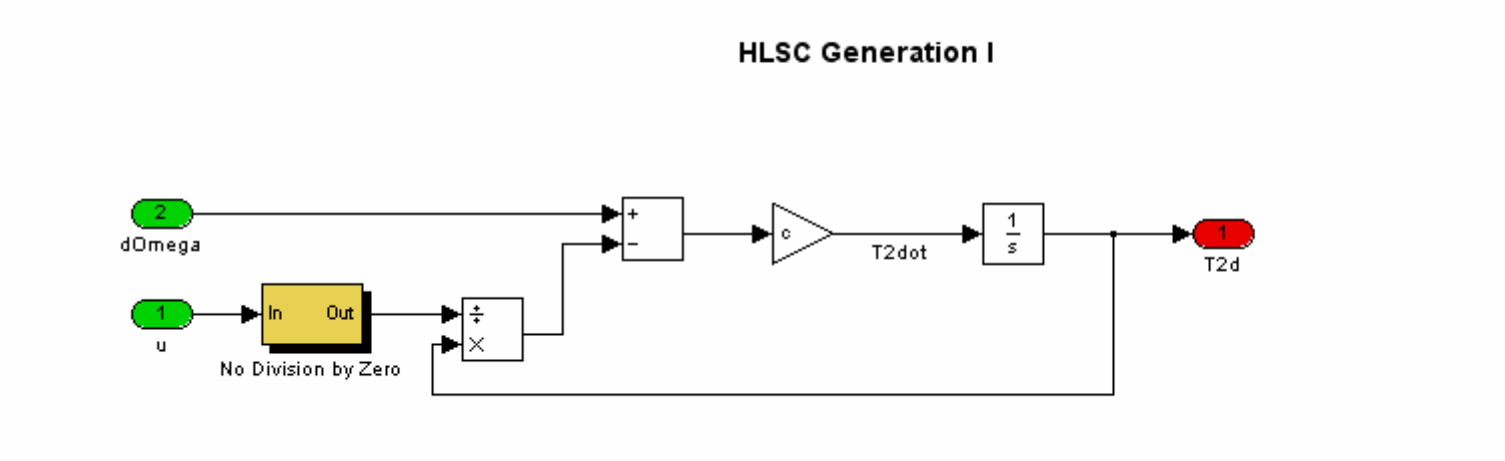

C.5.2 Generation IV

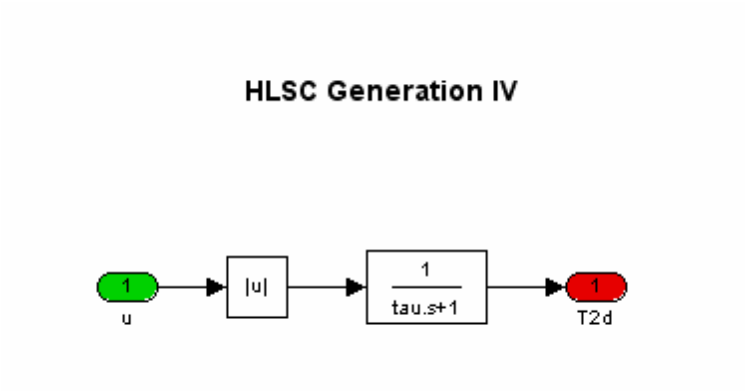

C.6 Controller

C.6.1 Anti-windup

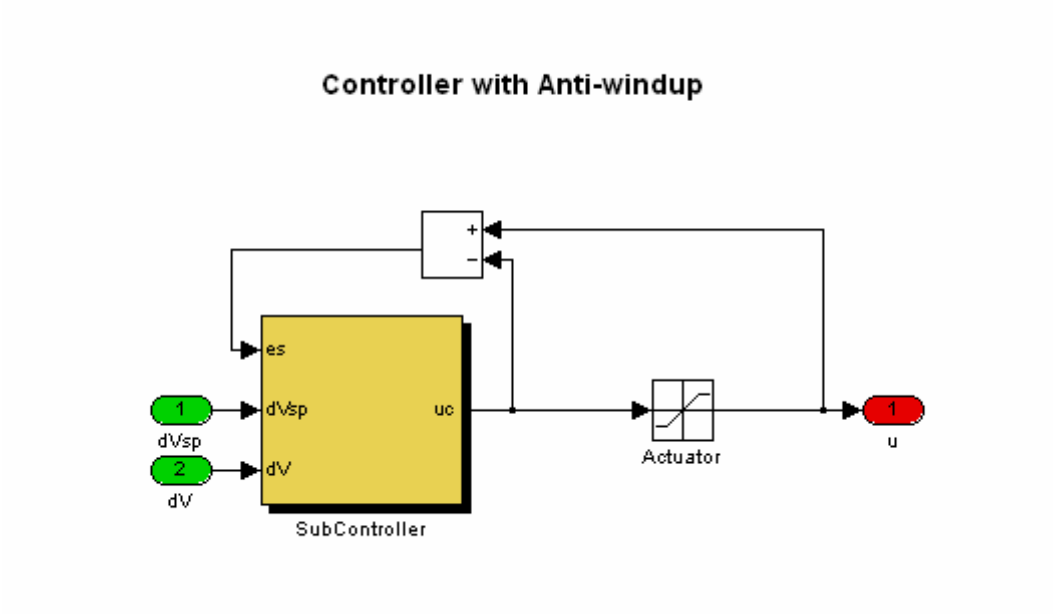

C.6.2 PID Controller